Origin of ureilites inferred from a SIMS oxygen isotopic and trace element study of clasts in the Dar al Gani 319 polymict ureilite

Noriko T. Kita,[1,†,*] Yukio Ikeda,[2] Shigeko Togashi,[1] Yongzhong Liu,[1,‡] Yuichi Morishita,[1] and Michael K. Weisberg[3,4]

[1]Geological Survey of Japan, AIST, AIST Central 7, Tsukuba 305-8567, Japan
[2]Faculty of Science, Ibaraki University, Mito 301-8512, Japan
[3]Department of Physical Sciences, Kingsborough College (CUNY), 2001 Oriental Boulevard, Brooklyn, NY 11235, USA
[4]Department of Earth and Planetary Sciences, American Museum of Natural History, New York, NY 10024, USA

Abstract—Secondary ion mass spectrometer (SIMS) oxygen isotope analyses were performed on 24 clasts, representing 9 clast types, in the Dar al Gani (DaG) 319 polymict ureilite with precisions better than 1‰. Olivine-rich clasts with typical ureilitic textures and mineral compositions have oxygen isotopic compositions that are identical to those of the monomict ureilites and plot along the CCAM (Carbonaceous Chondrite Anhydrous Mineral) line. Other igneous clasts, including plagioclase-bearing clasts, also plot along the CCAM line, indicating that they were derived from the ureilite parent body (UPB). Thus, we suggest that some of the plagioclase-bearing clasts in the polymict ureilites represent the "missing basaltic component" produced by partial melting on the UPB.

Trace element concentrations (Mg, K, Sc, Ti, V, Cr, Mn, Fe, Co, Ni, Cu, Rb, Sr and Ba) in ureilitic plagioclase and glass from 13 clasts were obtained by using the SIMS high mass resolution method. The trace element contents of the plagioclase generally show monotonic variations with anorthite content (mol%) that are consistent with partial melting and fractional crystallization. Incompatible trace element concentrations (K, Ti, and Ba) are low and variable for plagioclase with An > 40, indicating that the parental magmas for some clasts were derived from a depleted source. We performed partial melt modeling for CI and CM precursor compositions and compared the results to the observed trace element (K, Ba, and Sr) abundances in the plagioclase. Our results indicate that (1) the UPB evolved from a alkali-rich carbonaceous chondritic precursor, (2) parent melts of porphyritic clasts could have formed by 5–20% equilibrium partial melting and subsequent fractional crystallization, and (3) parent melts of the incompatible trace element-depleted clasts could be derived from fractional melting, where low degree (<10%) partial melts were repeatedly extracted from their solid sources.

Thus, both the oxygen isotopic and trace element compositions of the plagioclase bearing clasts in DaG-319 suggest that the UPB underwent localized low degree-partial melting events. The partial melts could have been repeatedly extracted from the precursor, resulting in the formation of the olivine-pigeonite monomict ureilites as the final residue. *Copyright © 2004 Elsevier Ltd*

1. INTRODUCTION

Most ureilites are olivine-pigeonite ultramafic rocks with highly depleted REE abundances, indicating that the ureilite parent body (UPB) underwent extensive igneous processing (Boynton et al., 1976; Berkley et al., 1980; Goodrich and Jones, 1987; Goodrich, 1992). Oxygen isotopes in the ureilites do not follow a single mass fractionation line, but plot along a mixing line between CAIs, dark inclusions and matrix in carbonaceous chondrites, which is called the Carbonaceous Chondrite Anhydrous Mineral (CCAM) line (Clayton and Mayeda, 1988). The magnesian numbers (hereafter mg#; molar [MgO]/[MgO + FeO] %) in individual ureilites correlate with ^{16}O enrichment, similar to the relationship between the mg# of olivine-pyroxene and the bulk oxygen isotopic compositions for equilibrated ordinary chondrites (Clayton and Mayeda, 1991).

Furthermore, olivine-pigeonite ureilites contain carbon-metal veins with abundant trapped noble gasses that show the lowest $^{40}Ar/^{36}Ar$ ratios observed in meteoritic materials (Göbel et al., 1978). These "primitive" features are difficult to explain if the UPB experienced planetary scale differentiation. To reconcile these difficulties, many authors proposed that the ureilites formed as partial melt residues of a chondritic precursor (Warren and Kallemeyn, 1992; Scott et al., 1993). Yet, equilibrium partial melting calculations indicate that a chondritic precursor will not produce an olivine-pigeonite residue unless it is enriched in Ca relative to Al, but instead result in an olivine-orthopyroxene residue (Goodrich, 1999). Smelting experiment by Singletary and Grove (2003) indicated that ureilites are the residue of partial melting/smelting events and mg# of ureilites might inversely correlate with the smelting depth. However, this model raised the question of whether the UPB accreted selectively from ^{16}O depleted to enriched precursors in accordance with the observed ^{16}O-enrichment and mg# correlation. These difficulties left the origin of ureilites as one of the major unsolved issues in meteoritical studies.

The absence of basaltic meteorites related to the olivine-pigeonite ureilites is another perplexing problem in understanding ureilite petrogenesis. It was suggested that the "missing

* Author to whom correspondence should be addressed (noriko.kita@aist.go.jp).
† *Present address:* Department of Geology and Geophysics, University of Wisconsin, 1215 W. Dayton Street, Madison, Wisconsin 53706-1692, USA.
‡ *Present address:* Department of Earth and Environmental Sciences, University of Rochester, Hutchison Hall 227, Rochester, NY 14627, USA.

basalt" was lost from the parent body by explosive volcanism or planetary collisions (Takeda, 1987; Warren and Kallemeyn, 1989, 1992; Scott et al., 1993). Several polymict ureilites have been recognized to contain plagioclase-bearing clasts (Jaques and Fitzgerald, 1982; Prinz et al., 1983, 1986, 1987). However, the origin of these clasts is not clear, as they contain plagioclase with a wide range of anorthite contents, from 0 to 100%, and may also include exotic materials. For example, in addition to plagioclase of possible ureilitic origins, pure anorthite, similar to that in some angrites, and albitic plagioclase, similar to that from ordinary chondritic materials, have been observed (Prinz et al., 1986). Because of these diverse compositions and a scarcity of samples, as well as small sample size of the clasts and the fact that most clasts are incomplete mineral assemblages, studies on the basaltic components from the UPB are limited. Guan and Crozaz (2001) studied REE abundances in plagioclase and melt clasts in polymict ureilites and concluded that these clasts formed by 20–30% partial melting of a chondritic precursor. However, the diversity of REE abundances in the plagioclase cannot be the result of a single igneous differentiation process, but requires multiple processes.

Dar al Gani (DaG) 319 is a newly recognized polymict ureilite containing a variety of clasts including abundant plagioclase (Ikeda et al., 2000; Ikeda and Prinz, 2001). It contains various types of sub-mm to cm-sized lithic clasts, including: (1) "type I ureilitic clasts" similar to the monomict olivine-pigeonite ureilites, (2) "type II ureilitic clasts" consisting mainly of olivine and orthopyroxene, free of carbon-metal veins, and in some cases, containing magmatic inclusions (Ikeda and Prinz, 2001) that are similar to the unusual melt-inclusion-bearing monomict ureilite Hughes 009 (Goodrich et al., 2001), (3) felsic clasts with plagioclase compositions between An_0 and An_{100}, and (4) a variety of chondritic materials. Ikeda et al. (2000) proposed that the type I ureilitic clasts are the fragments of monomict ureilitic material, whereas type II ureilitic clasts and felsic clasts are derived from primary basaltic partial melts of the ureilitic precursor. They considered the type II clasts and felsic clasts to be cumulates and felsic magmas, respectively, produced during fractional crystallization of the primary magma. The major goals of this study are (1) to better characterize the various clasts and test their relationship to the monomict ureilites, by using in situ oxygen isotope analyses, and (2) to better understand igneous processes on the UPB by studying trace element abundances in ureilitic plagioclase.

For the purpose of identifying the clasts with ureilitic oxygen signature, the high precision (<1‰) oxygen isotopic data from tiny crystals (<20 μm) contained in mm-sized clasts are required. The current method of SIMS and laser probe oxygen isotope analyses could not be applied, because they are limited either by precision (~2‰ for SIMS) or by spatial resolution (~50 μm for laser probe). Therefore, a method of high precision SIMS oxygen isotopic analysis using multicollection Faraday cups was newly developed for this study. Oxygen isotopic compositions of the chondritic clasts in DaG-319 were also measured, but are reported in a separate paper (Ikeda et al., 2003). The chondritic clasts also contain plagioclase as an interstitial phase, but their oxygen isotopic compositions clearly indicate that they are ordinary chondritic materials and not related to the ureilites.

2. SAMPLES AND ANALYTICAL METHOD

2.1. Samples and Electron Microprobe Analyses

We studied 32 clasts from three thin sections of DaG-319 (AMNM 4963-1, 4963-2, 4963-3, which are denoted as "α," "β," and "γ," respectively), as shown in Table 1. Among them, 24 clasts were measured for oxygen isotope, and 13 clasts (felsic and glassy clasts and plagioclase fragments) for trace element analyses. Detailed petrographic descriptions and electron microprobe analyses of all clasts were made prior to the SIMS analyses. Petrographic descriptions of most clasts are reported in Ikeda et al. (2000) and Ikeda and Prinz (2001). Additional analyses were made using the electron-probe micro-analyzer (EPMA) for minerals and glass in clasts that were not described previously. A sample current of 3–5 nA, accelerating voltage of 15 kV, and measurement time of 10 seconds for peak and background were adopted. Corrections were carried out by the Bence and Albee method. Detailed analytical conditions are described in Ikeda and Prinz (2001). Classification of these clasts follows that of Ikeda et al. (2000) and is briefly described here.

2.1.1. Type I ureilitic clasts and related olivine fragments

Type I ureilitic clasts are similar to monomict ureilites showing characteristic carbon-metal veins and reduction olivine rims (Fig. 1a). Their olivine core compositions are between Fo75–85. We studied six olivine fragments for oxygen isotopes.

2.1.2. Type II ureilitic clast

Type II clast γ1 consists of olivine, orthopyroxene and augite without carbon-metal vein and contains magmatic inclusions (Ikeda and Prinz, 2001; Fig. 1b). It is more magnesian (mg# of olivine cores is ~88) than type I ureilitic clasts and it resembles the unusual monomict ureilite Hughes 009 (Goodrich et al., 2001).

2.1.3. Magnesian olivine-rich clasts and magnesian mineral fragment

These clasts and fragments consist of mafic minerals with higher mg# of 88–100. Some of them are similar to magnesian monomict ureilites (α37A shown in Fig. 1c, α8D and α3A), or to type II ureilitic clasts (α20A). Nearly pure forsterite fragments were also found (α23A), which are not similar to olivine in any known monomict ureilites.

2.1.4. Fine grained mafic lithic clast

In contrast to coarse grained texture of the ureilitic clasts, the fine-grained mafic lithic clasts have finer textures, possibly formed by shock-induced brecciation and subsequent recrystallization or by shock melting and rapid cooling of ureilitic materials. The fine-grained granular olivine-rich clast α8B consists of olivine with minor low Ca-pyroxene and alkali-free interstitial glass (Ikeda et al., 2000).

2.1.5. Porphyritic felsic clasts, plagioclase fragments, and gabbroic clast

Porphyritic felsic clasts, plagioclase fragments, and gabbroic clasts contain plagioclase with igneous textures (Figs. 1d–i). Detailed descriptions of these clasts are reported in Ikeda et al. (2000) and Ikeda and Prinz (2001). Cohen et al. (2004) reported similar clasts in DaG-319 and other polymict ureilites. They have a wide range of plagioclase (An0–100) and mafic mineral (mg# are 50–99) compositions, indicating a variety of parental magma compositions. The plagioclase-bearing clasts show systematic changes in their texture with An contents (Ikeda et al., 2000). Clasts with albitic to oligoclase plagioclase (An0–20) have porphyritic texture, containing pyroxene and plagioclase phenocrysts with phosphates and ilmenites as accessory minerals and a fine-grained albitic groundmass (α19A, α21A, α34A, γ5, γ15). Clasts having oligoclase to labradoritic plagioclase (An20–60) have a coarser porphyritic texture (α32C, α13A). Some porphyritic clasts show reverse zoning between pyroxene phenocrysts and surrounding rim (Figs.

Table 1. List of clasts in DaG-319 measured by SIMS.[a]

Clast	Classification	Mineral	mg#	Oxygen	Trace	Ref.
Type I ureilitic clasts and related olivine fragments						
α7A	ureilitic olivine fragment	Fo_{75}	75	Ol		
α9A	ureilitic olivine fragment	Fo_{76}	76	Ol		
α20C	ureilitic olivine fragment	Fo_{77}	77	Ol		
α18C	ureilitic olivine fragment	Fo_{78}	78	Ol		
α31A	ureilitic olivine fragment	Fo_{80}	80	Ol		
α18B	ureilitic olivine fragment	Fo_{83}	83	Ol		1
Type II ureilitic clast						
γ1	olivine-orthopyroxene-augite	Fo_{88}, $Wo_5En_{84}Fs_{11}$, $Wo_{37}En_{57}Fs_6$	88	Ol, Opx		1,2
Magnesian olivine-rich clast						
α37A	magnesian olivine-orthopyroxene	Fo_{97}, $Wo_5En_{93}Fs_2$	97	Ol		1
Magnesian mineral fragments						
α8D	magnesian ureilitic olivine fragment	Fo_{88}	88	Ol		
α3A	magnesian ureilitic olivine fragment	Fo_{92}	92	Ol		
α20A	orthopyroxene	$Wo_4En_{88}Fs_8$	92	Opx		1
α23A	forsterite	Fo_{100}	100	Ol		
Fine grained mafic lithic clast						
α8B	fine grained granular olivine-rich type	Fo_{79}	79	Ol		1
Porphyritic felsic clasts and plagioclase fragments						
γ18	plagioclase	An_{93-96}			P1	
β34A	plagioclase (with augite inclusion)	An_{92-93}, $Wo_{48}En_{51}Fs_1$	97	P1		
α32C	porphyritic (pigeonite, plagioclase, augite, chromite)	$Wo_{14}En_{44}Fs_{42}$, An_{36-60}, $Wo_{25}En_{28}Fs_{47}$	51		P1	
α22A	plagioclase (with magmatic inclusion)	An_{47}	87*[1]	P1	P1	1,2
α23B	plagioclase	An_{36-38}				
α20B	plagioclase	An_{28-40}			Pl	
α13A	porphyritic (augite, plagioclase)	$Wo_{38}En_{46}Fs_{16}$, An_{11-22}	74	Aug	Pl	1
γ5	porphyritic (plagioclase, augite, pigeonite, apatite)	An_{11-17}, $Wo_{37}En_{47}Fs_{16}$, $Wo_{28}En_{63}Fs_9$	70–75		Pl	2
α34A	porphyritic (plagioclase, pigeonite, augite, whitlockite)	An_{3-21}, $Wo_{10}En_{53}Fs_{37}$, $Wo_{37}En_{48}Fs_{15}$	59, 76	Pl, Pig	Pl	1,2
α19A	porphyritic (augite, plagioclase, ulvöspinel)	$Wo_{37}En_{49}Fs_{14}$, An_{2-10}	77		Pl	
γ15	porphyritic (plagioclase, augite, pig-eonite, whitlockite, apatite, ilmenite)	An_{2-9}, $Wo_{38}En_{38}Fs_{24}$, $Wo_9En_{46}Fs_{45}$	50–60		Pl, G	1
α21A	porphyritic (plagioclase, glass)	An_{2-4}	11*[2]		Pl, G	
Gabbroic clasts						
γ8	troctolitic (plagioclase, olivine)	An_{87-89}, Fo_{93}	93	Ol	Pl	1
α21B	anorthite-fassaite	An_{99}, $Wo_{49}En_{35}Fs_{16}$	68	Aug		1
Glassy clasts						
α8A	magnesian glassy clast	$Wo_{0.9}En_{98.5}Fs_{0.6}$	99	Opx	G	1
α16A	ferroan glassy clast	Fo_{82-86}, $Wo_1En_{79}Fs_{20}$	79	Ol	G	1
Dark clasts						
γ3	enstatite in dark clast	En_{100}	100	Opx		1
β9B	Fa-free dark clast			Mt		
α27A	lithic fragments and fayalite in Fa-bearing dark clast	Fo_{1-99}	1–99	Ol		1

[a] The classifications of clasts are after Ikeda et al. (2000). Column "mg#" indicates molar MgO/(MgO+FeO) % in major mafic minerals in individual clasts. The columns "Oxygen" and "Trace" indicate the phases used for SIMS oxygen and trace element analyses, respectively. "Ol", "Opx", "Pig", "Aug", "Pl", "G", and "Mt" represent olivine, orthopyroxene, pigeonite, augite, plagioclase, glass, and magnetite, respectively. *[1]Pyroxene in magmatic inclusion, *[2]Data obtained from glass. Reference numbers correspond to [1] Ikeda at al. (2000) and [2] Ikeda and Prinz (2001).

1d,g); augite (mg#74) is surrounded by a diopside rim in α13A and pigeonite (mg#59) is surrounded by a magnesian augite rim (mg#76) in α34A (Ikeda et al., 2000). Andesine to anorthitic plagioclase occurs as isolated mineral fragments and in gabbroic clasts. The plagioclase compositions of these fragments and clasts are nearly homogeneous. One large plagioclase fragment α22A (An47; Fig. 1f) contains magmatic inclusions with zoned sodic plagioclase (<An40; Ikeda and Prinz, 2001). One of the gabbroic clasts α21B (Fig. 1i) consists of anorthite and fassaite, which is similar to the angritic clasts described by Prinz et al. (1987).

2.1.6. Glassy clasts

Glassy clasts consist of phenocrysts of olivine and/or pyroxene included in a SiO_2-rich glass (SiO_2 = 60–70%). A magnesian glassy clast, α8A, consists mainly of enstatite phenocrysts and needle-like diopside set in magnesian glass, where a ferroan clast, α16A, includes olivine and orthopyroxene set in ferroan glass.

2.1.7. Minerals and lithic fragments in dark clasts

DaG-319 contains CI-like chondritic dark clasts with hydrous silicates and/or fayalite and magnetite (Ikeda et al., 2000, 2003). Some of these clasts contain exotic unaltered, anhydrous minerals in a phyllosilicate-rich matrix (e.g., an enstatite grain was found in the fayalite-free dark clast γ3.) Fayalite-free dark clast β9B contains fine grained framboidal magnetites, which are aggregates of tiny (<10 μm) spherules. The fayalite-bearing dark clast α27A contains variety of mafic lithic fragments, including olivine and pyroxene with peridotic or
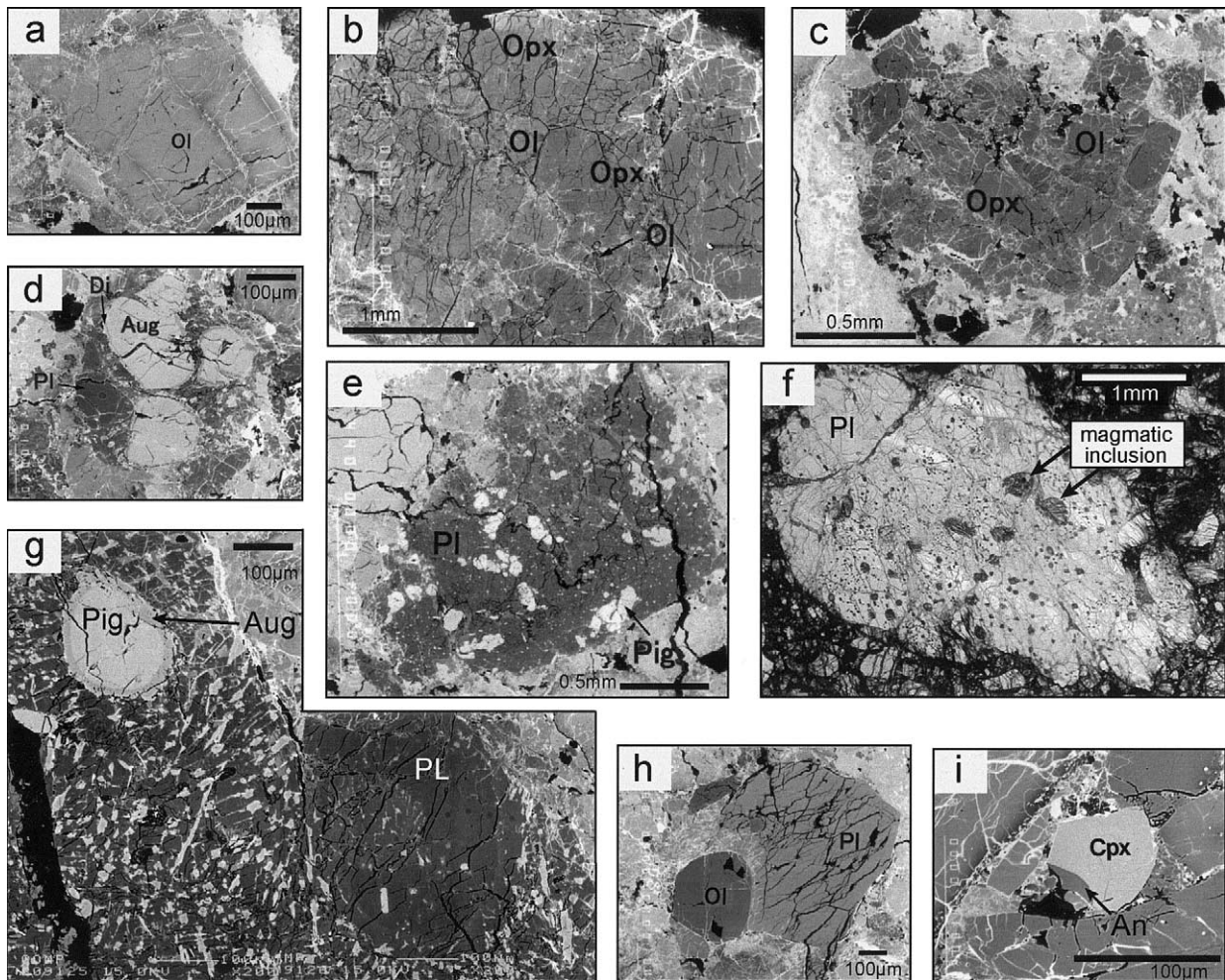
Fig. 1. Photographs of igneous clasts in DaG-319. Back scattered electron (BSE) photographs, unless otherwise indicated. (a) Type I clast α18B (olivine fragment) with typical ureilitic carbon-metal veins. (b) Type II clast γ1 without carbon-metal vein. (c) Magnesian olivine-rich clast α37A. (d) Porphyritic felsic clast α13A. (e) Porphyritic felsic clast γ15. (f) Plagioclase fragment α22A with magmatic inclusions, transmitted light. (g) Porpyritic felsic clast α34A, showing reverse zoned pyroxene and plagioclase phenocryst. (h) gabbroic clast γ8. (i) gabbroic clast α21B with angritic composition.

basaltic compositions (Ikeda et al., 2000). The groundmass of the lithic fragments is generally rich in hydrous phyllosilicates.

2.2. Oxygen Isotope Analyses

For the purpose of identifying the origin of the various clasts in DaG-319, we needed to obtain oxygen isotopic data with a precision better than 1‰. In current SIMS oxygen three-isotope measurements, the most abundant isotope, ^{16}O, is detected with a Faraday cup (FC) detector, while the other two isotopes, ^{17}O and ^{18}O, are detected with an electron multiplier (EM) in pulse counting mode (Choi et al., 1997), because of their low isotopic abundances of 0.04% and 0.2%, respectively. This method introduces an uncertainty of ~2‰ on the measured isotopic ratios from the calibration of the two different detectors. For this reason, we decided to use three FCs simultaneously by using the multicollection system of the IMS-1270 at the Geological Survey of Japan (GSJ). This is advantageous because the relative sensitivities among the different FC detectors are highly stable ($\leq$0.1‰) over a long period.

The 0.7–0.9 nA Cs+ primary ion beam (20 keV total acceleration voltage) was shaped to a diameter of 12 μm on the sample surface, and the secondary O^- ions were accelerated by -10 kV under the electron gun for charge compensation. Three isotopes of oxygen are detected

simultaneously by combination of two multicollector FCs (^{16}O and ^{18}O) and a mono-collector FC (^{17}O) on the axial position. The intensity of ^{16}O was typically ~8 $\times$ 10^8 cps. The mass resolving power (MRP) was set to 4500 for the axial detector to separate ^{16}OH interference from ^{17}O, while those of ^{16}O and ^{18}O were 2000 that were enough to separate molecular interferences. The contribution of ^{16}OH on ^{17}O is in the range of 10^{-5}. An interference correction was made in a few cases where the analyzed surface included cracks or grain boundaries with abundant ^{16}OH signals from adsorbed water higher than 10 times the ^{17}O signals. The internal precision of a single analysis (40 cycles, ~25 min) yielded 0.3‰ and ~1‰ (2σ) for ($^{18}O/^{16}O$) and ($^{17}O/^{16}O$) ratios, respectively. More detailed descriptions of the analytical condition are in Appendix 1.

We carried out analyses in three analytical sessions; in May 2000, July–August 2000 and March 2001. Terrestrial standard data are shown in detail in Appendix 2. The instrumental mass fractionation effect is corrected using terrestrial standards of olivine (Fo$_{90}$, Fo$_{60}$), orthopyroxene (En$_{90}$), diopside, plagioclase (An$_{95}$ and An$_{30}$), and magnetite. Measured $^{18}O/^{16}O$ and $^{17}O/^{16}O$ ratios are normalized by using Standard Mean Ocean Water compositions (SMOW) and are corrected for the instrumental mass fractionation factor f of each mineral, as follows:

$$\delta^{18}O = \left(\frac{(^{18}O/^{16}O)_{measured}}{(^{18}O/^{16}O)_{SMOW}} - 1\right) \times 1000 - f,$$

$$\delta^{17}O = \left(\frac{(^{17}O/^{16}O)_{measured}}{(^{17}O/^{16}O)_{SMOW}} - 1\right) \times 1000 - .52f,$$

where $(^{18}O/^{16}O)_{SMOW}$ is from the literature value of 0.0020052 (Baertschi, 1976) and $(^{17}O/^{16}O)_{SMOW}$ is the mean value obtained from the all the terrestrial standard analyses during the individual analytical sessions (see Appendix 2). The ^{16}O enrichments in meteorite samples are expressed as $\Delta^{17}O$ as,

$$\Delta^{17}O = \delta^{17}O - 0.52 \times \delta^{18}O.$$

In earlier analytical sessions, external reproducibility of measured $\delta^{18}O$ values for individual mineral standards is much larger than the internal errors (0.2–0.4‰). It ranges 0.6–2.0‰ and 0.3–1.1‰ (2σ) for each day in May 2000 and July–August 2000 sessions, respectively. Therefore, we assigned external errors of 1.5‰ and 0.5‰ for $\delta^{18}O$ values in May 2000 and July–August 2000 sessions, respectively. During the course of the study, we recognized that the careful tuning and spot to spot adjustment of the electron gun is a key to reduce the external error in $\delta^{18}O$ values. After we established a routine adjustment procedure for the electron gun in March 2001 (Appendix 1), repeated analyses of $\delta^{18}O$ in our terrestrial olivine standard agreed well within its internal errors. The external error of $\delta^{17}O$ values is assumed to be half of $\delta^{18}O$ values for each session. Only the internal errors are assumed for $\Delta^{17}O$ values, as the instrumental mass fractionation corrected $(^{17}O/^{16}O)_{SMOW}$ ratios among terrestrial standards do not indicate any external errors in each session (as shown in Appendix 2).

Repeated analyses of three olivine standards with different Fo contents do not show any systematic variation among their f values. However, there are systematic difference among pyroxene and plagioclase standards; diopside standards are always ~3‰ higher than orthopyroxene standards and anorthite standard (An$_{95}$) are ~1‰ higher than more albitic plagioclase (An$_{30}$). We linearly interpolated the matrix effects of f values according to Ca contents of pyroxene and An contents of plagioclase, by using these standard minerals.

In one case, we used a 25 μm beam size with a primary ion current of 2.5–3 nA, in order to achieve the high internal precision on $\delta^{17}O$ data (0.3‰) by using high secondary ^{17}O currents (~10^6 cps). As we did not examine reproducibility of f values in this condition, only the $\Delta^{17}O$ value is used for 25 μm beam size analysis. The average $(^{17}O/^{16}O)_{SMOW}$ ratios of terrestrial standards agree well with those of 12 μm beam size analyses in the same analytical session. This analytical condition allows us to determine the $\Delta^{17}O$ value of the meteoritic sample with the precision of 0.3‰ for a single analysis.

2.3. Plagioclase Trace Element Analyses

Eighteen major and trace elements (Na, Mg, Al, Si, K, Ca, Sc, Ti, V, Cr, Mn, Fe, Co, Ni, Cu, Rb, Sr, Ba) in plagioclase and glass were analyzed using SIMS. The analytical procedure is similar to that of Togashi et al. (2003). The sample surface was bombarded with a primary ion beam of O^- having an acceleration voltage of 23 kV, a 12 μm spot size, and an intensity of 0.5 nA. The field aperture was opened to cover the 25 μm square area on the sample surface and secondary ions were collected at a MRP of 4500. We did not apply energy filtering, as most of the molecular interferences including hydrides can be resolved from the analyzed ions. For one sample with low K content, a 25 μm primary ion beam was used and the field aperture was set to collect only the central 7 μm square area. This procedure reduced contamination of K from the edge of the sputtered crater. A single analysis normally took 20 min.

Terrestrial plagioclase standards (An$_{95}$-An$_{22}$), geological glass standards (peridotite, basalt, komatiite, andesite, rhyolite) from the Max-Planck Institute (Jochum et al., 2000) and a fused JB1a glass with known major and trace element concentrations (Imai et al., 1995) were used for calibrating secondary ion relative sensitivities. Isobaric interferences on ^{85}Rb, ^{88}Sr and ^{138}Ba were significantly large for peridotite glass standards with concentrations less than 1 ppm, which might be derived from SiFe and Mg_2FeO_2 molecular ions. For plagioclase analyses, these molecular ions produced by the combination of major

elements are insignificant as both Mg and Fe contents in plagioclase are much less than 1%. Peridotite glass standard also indicates small contributions of $^{40}Ca^{48}Ca$ and $^{44}Ca_2$ on ^{88}Sr, comparable to apparent Sr concentrations of 1 ppm. This interference may not affect plagioclase analyses as Sr concentrations are usually in the level of 100 ppm. Furthermore, $^{42}Ca^{43}Ca$ interference on ^{85}Rb is orders of magnitude smaller than those on ^{88}Sr because of low isotopic abundance of ^{42}Ca and ^{43}Ca. We estimated the contribution of $^{42}Ca^{43}Ca$ interference on ^{85}Rb to be less than 0.003 ppm.

The SIMS relative sensitivity factors (RSF) for Ti, Mn, Fe and Ba in the oligoclase standard (An$_{22}$) and Ba in the anorthite standard (An$_{95}$) were significantly lower than the other standards, while those for other trace elements (Mg, Co, Sc, Sr) agree within 30%. The discrepancy may be due to tiny inclusions of other minerals that caused higher bulk concentrations of these elements in the standards, or due to the uncertainty of analyzing a small sample size by ICP-MS. Excluding these data, the average SIMS sensitivity factor was calculated for each element relative to Si. We did not notice significant matrix effects among the plagioclase standards. However, there were systematic variations in sensitivity factors with SiO$_2$ contents among the glass standards (up to a factor of 2 for some elements). This matrix effect was taken into consideration when we calculated the trace element concentrations in unknown glass samples. The concentrations of V, Cr, Cu, Ni, and Rb in the plagioclase standards were not known. We found constant ratios of RSF for V/Ti, Cr/Mn, Cu/Fe, Ni/Fe, and Rb/K in glass standards. Assuming plagioclase standards have similar RSF ratios, we inferred the RSFs for V, Cr, Cu, Ni, and Rb in plagioclase from RSF ratios in glass standards. For this reason, concentrations of V, Cr, Cu, Ni and Rb in plagioclase should be considered as semi-quantitative values.

3. OXYGEN ISOTOPIC RESULTS

3.1. ALH 77257 Monomict Ureilite

To evaluate our SIMS measurements, we analyzed one Antarctic monomict ureilite, ALH 77257 (a thin section made from a chip of NIPR ALH-77257, 79). Clayton and Mayeda (1988, 1996) measured the same meteorite previously by using their standard dissolution technique. The results of repeated analyses are shown in Table 2. Compared to the whole rock composition reported by Clayton and Mayeda (1988, 1996), our results appear to be fractionated toward heavy isotopes along a (slope 0.5) mass fractionation line by ~1‰ (Fig. 2). It is interesting to note that our SIMS results plot right on the CCAM line (Fig. 2), which most monomict ureilites follow and the ALH 77257 data of Clayton and Mayeda (1988, 1996) do not. Clayton and Mayeda (1988) pointed out that the Antarctic ureilites might be contaminated by an Antarctic water component ($\delta^{18}O \sim -40‰$). Their samples that were not acid washed to remove terrestrial weathering products may be shifted along a slope 0.5 line because the mixing line between the ureilite data on the CCAM line and the Antarctic water component is nearly parallel to a mass fractionation line. Using SIMS, we analyzed the center of the olivine grains, so that we were able to avoid grain boundaries where most of the weathered components might be located. Therefore, we infer that our SIMS data represent the true value for the meteorite.

As described earlier, our data from May 2000 show a larger variation in $\delta^{18}O$ (Table 2) because of analytical uncertainty related to electron gun adjustment. The statistical evaluation using the ISOPLOT program (Ludwig, 1999) indicated an external error of 0.6‰ for the $\delta^{18}O$ data of May 2000. Nevertheless, the averages of the two analytical sessions agree with each other well within the analytical uncertainty of 0.3‰ (Fig. 2).

Table 2. Oxygen isotopic analyses of olivine in ALH-77257 monomict ureilite.[a]

Analyses session	Mineral	$\delta^{18}O$	Error (2σ)	$\delta^{17}O$	Error (2σ)	$\Delta^{17}O$	Error (2σ)
May 2000	olivine	7.7	0.2	2.8	0.9	−1.2	0.9
	olivine	6.8	0.3	3.1	1.1	−0.4	1.1
	olivine	7.5	0.3	2.9	1.1	−1.1	1.1
	olivine	7.5	0.2	3.4	1.2	−0.5	1.2
	olivine	7.3	0.2	2.4	0.9	−1.4	1.0
	average	7.4	0.3	2.8	0.5	−1.0	0.5
	external error		0.6				
August 2000	olivine	7.6	0.2	3.5	1.2	−0.5	1.2
	olivine	7.8	0.3	2.5	1.2	−1.6	1.2
	average	7.7	0.2	3.0	0.8	−1.0	0.8
Literature data[b]	bulk	6.91		2.51		−1.08	0.08
	bulk	6.30		2.38		−0.90	0.08
	average	6.61		2.45		−0.99	

[a] The errors equated for individual analyses are internal errors ($2\sigma_{mean}$) only. The average of each session and its errors are calculated by considering external errors (using the ISOPLOT program by Ludwig, 1999). The error of average $\delta^{18}O$ value in the 2000 May session exceeds the internal error of the individual analysis, indicating a large external error.

[b] Literature data are from Clayton and Mayeda (1988), (1996).

3.2. DaG-319 clasts

The results of oxygen isotope analyses for clasts and fragments in DaG-319 are shown in Table 3, and Figures 3 and 4. In some clasts, the secondary ^{16}O intensity decreased more than 50% with time in a single analysis and measured $\delta^{18}O$ and $\delta^{17}O$ values gradually decreased (>10‰ for $\delta^{18}O$). This type of unusual run happened only for the fine-grained dark clasts or the nearly FeO-free minerals, indicating that sample charging effects are the main cause of unstable data. As the measured $\delta^{18}O$ and $\delta^{17}O$ values moved along a mass fractionation line

Fig. 2. SIMS oxygen isotope analyses of ALH 77257 olivine. The mean values in Table 2 are shown. The error bars represent standard error of the mean (2σ). Two bulk analyses (solid diamonds) from Clayton and Mayeda (1988, 1996) are shown for reference; these might be contaminated with Antarctic water. "T.F." and "CCAM" indicate the terrestrial mass fractionation line and carbonaceous chondrite anhydrous mineral mixing line, respectively.

during the single measurement, only $\Delta^{17}O$ values were obtained and are shown in Table 4.

3.2.1. Type I ureilitic clasts

All the type I ureilitic clasts studied here plot along the CCAM line within error (Fig. 3a). The diagram of mg# versus $\Delta^{17}O$ in Figure 4 indicates that the type I ureilitic clasts show the same relationships as monomict ureilites. These clasts represent fragments of monomict-ureilitic samples.

3.2.2. Olivine-orthopyroxene-augite (type II) clasts

Olivine and orthopyroxene in the type II ureilitic clast γ1 were measured and plot near the CCAM line, as in the case of the type I ureilitic clasts (Fig. 3b). Since this sample was measured in May 2000 analytical session, the individual orthopyroxene data scatter due to poor reproducibility in the measured $\delta^{18}O$. There are no detectable differences in $\delta^{18}O$ values between olivine and orthopyroxene, indicating that the oxygen isotopic fractionation between olivine and pyroxene is smaller than 0.5‰. The $\Delta^{17}O$ values of these clasts are ~−1‰ (Fig. 4) and plot within the range of the monomict ureilite trend. Even though there are large uncertainties in our oxygen isotope data, it should be noted that the data for γ1 on Figure 4 plot very closed to the position of Hughes 009 (Clayton and Mayeda, 1996), an unusual monomict ureilite similar to γ1 in petrology and mineral chemistry (Goodrich et al., 2001; Ikeda and Prinz, 2001).

3.2.3. Magnesian olivine-rich clast, magnesian mineral fragments, and fine-grained mafic lithic clast

Clast α37A contains highly magnesian olivine and orthopyroxene (mg#~97). Magnesian olivine fragments (α3A and α8D; Fo$_{88-92}$) do not contain the typical ureilitic carbon-metal veins. Their oxygen isotopic compositions are identical to the monomict ureilites with similar mg#, showing the same mg#-$\Delta^{17}O$ relationship characteristic of the monomict ureilites (Figs. 3c and 4). The oxygen isotopic composition of the

Table 3. SIMS oxygen isotopic analyses of minerals in DaG-319 clasts.[a]

Sample	Mineral	Session	$\delta^{18}O$ error (2σ)	$\delta^{17}O$ error (2σ)	$\Delta^{17}O$ error (2σ)
Type I ureilitic clasts and related olivine fragments					
α7A	olivine	2000 Aug	7.8 $\pm$ 0.6	3.7 $\pm$ 1.3	-0.4 ± 1.3
α9A	olivine	2000 Aug	8.6 $\pm$ 0.5	3.9 $\pm$ 1.1	-0.5 ± 1.1
α20C	olivine	2000 July	8.8 $\pm$ 0.8	5.2 $\pm$ 2.6	0.7 $\pm$ 2.6
	olivine	2000 Aug	8.0 $\pm$ 0.5	2.5 $\pm$ 1.2	-1.7 ± 1.1
	olivine	2000 Aug	7.7 $\pm$ 1.6	4.5 $\pm$ 0.9	0.5 $\pm$ 1.2
	olivine	2000 Aug	8.4 $\pm$ 0.6	4.1 $\pm$ 0.8	-0.3 ± 0.7
	mean		8.3 $\pm$ 0.3	3.9 $\pm$ 1.1	-0.4 ± 1.1
α18C	olivine	2000 May	8.8 $\pm$ 1.5	4.7 $\pm$ 1.4	0.2 $\pm$ 1.2
α31A	olivine	2000 July	8.1 $\pm$ 0.6	3.5 $\pm$ 1.0	-0.8 ± 1.0
α18B	olivine	2000 May	7.8 $\pm$ 1.5	2.7 $\pm$ 1.4	-1.4 ± 1.2
Type II ureilitic clast					
γ1	olivine	2000 May	7.2 $\pm$ 1.5	3.2 $\pm$ 1.3	-0.5 ± 1.1
	opx	2000 May	6.2 $\pm$ 1.5	2.0 $\pm$ 1.2	-1.2 ± 0.9
	opx	2000 May	7.7 $\pm$ 1.5	2.8 $\pm$ 1.3	-1.2 ± 1.1
	opx	2000 May	6.5 $\pm$ 1.5	2.1 $\pm$ 1.2	-1.3 ± 0.9
	mean opx		6.8 $\pm$ 0.9	2.3 $\pm$ 0.7	-1.3 ± 0.6
Magnesian olivine-rich clasts					
α37A	opx	2000 Aug	4.4 $\pm$ 0.6	-1.1 ± 1.1	-3.3 ± 1.1
	opx[b]	2000 Aug	5.2 $\pm$ 0.1	0.2 $\pm$ 0.3	-2.5 ± 0.3
	mean		4.4 $\pm$ 0.6	-0.3 ± 0.3	-2.5 ± 0.3
Magnesian mineral fragments					
α8D	olivine	2000 Aug	5.6 $\pm$ 0.6	0.5 $\pm$ 1.4	-2.4 ± 1.4
	olivine	2000 Aug	5.3 $\pm$ 0.5	1.1 $\pm$ 0.9	-1.7 ± 0.9
	mean		5.5 $\pm$ 0.4	1.0 $\pm$ 0.8	-1.9 ± 0.7
α3A	olivine	2000 May	3.7 $\pm$ 1.5	0.4 $\pm$ 1.2	-1.5 ± 1.0
	olivine	2000 Aug	5.3 $\pm$ 0.6	0.4 $\pm$ 1.6	-2.4 ± 1.6
	mean		5.3 $\pm$ 0.6	1.1 $\pm$ 0.9	-1.7 ± 0.8
α20A	opx	2000 Aug	8.3 $\pm$ 0.5	2.2 $\pm$ 1.4	-2.1 ± 1.4
	opx	2000 Aug	8.1 $\pm$ 0.6	3.6 $\pm$ 1.2	-0.6 ± 1.2
	mean		8.2 $\pm$ 0.4	3.0 $\pm$ 0.9	-1.2 ± 0.9
α23A	forsterite	2000 Aug	5.8 $\pm$ 0.6	3.1 $\pm$ 1.1	0.1 $\pm$ 1.0
Fine grained mafic lithic clasts					
α8B	olivine	2000 Aug	8.3 $\pm$ 0.7	3.4 $\pm$ 0.8	-0.9 ± 0.9
	olivine	2000 Aug	7.8 $\pm$ 0.6	3.5 $\pm$ 1.1	-0.5 ± 1.1
	mean		8.0 $\pm$ 0.5	3.4 $\pm$ 0.7	-0.8 ± 0.7
Porphyritic felsic clasts and plagioclase fragments					
β34A	plagioclase	2000 Aug	8.5 $\pm$ 0.6	3.9 $\pm$ 1.1	-0.5 ± 1.1
α22A	plagioclase	2000 Aug	9.0 $\pm$ 0.6	4.3 $\pm$ 1.1	-0.4 ± 1.1
α13A	augite	2000 Aug	7.1 $\pm$ 0.8	3.1 $\pm$ 1.3	-0.6 ± 1.3
	augite	2000 Aug	7.0 $\pm$ 0.8	3.1 $\pm$ 1.4	-0.6 ± 1.4
	mean		7.1 $\pm$ 0.6	3.1 $\pm$ 1.0	-0.6 ± 1.0
α34A	plagioclase	2000 Aug	7.4 $\pm$ 0.6	2.5 $\pm$ 1.0	-1.4 ± 1.0
	pigeonite	2000 Aug	7.1 $\pm$ 0.6	1.9 $\pm$ 1.0	-1.7 ± 1.0
Gabbroic clasts					
γ8	olivine	2000 May	7.7 $\pm$ 1.6	2.2 $\pm$ 1.1	-1.8 ± 0.8
	olivine	2000 May	7.4 $\pm$ 1.5	2.6 $\pm$ 1.2	-1.2 ± 0.9
	mean		7.5 $\pm$ 1.1	2.4 $\pm$ 0.8	-1.6 ± 0.6
α21B	fassaite	2000 Aug	3.8 $\pm$ 1.0	1.9 $\pm$ 1.2	-0.1 ± 1.3
	fassaite	2000 Aug	4.6 $\pm$ 0.9	1.2 $\pm$ 1.6	-1.2 ± 1.6
	mean		4.2 $\pm$ 0.7	1.7 $\pm$ 1.0	-0.5 ± 1.0
Glassy clasts					
α8A	En	2000 Aug	4.1 $\pm$ 0.7	1.2 $\pm$ 1.0	-1.0 ± 0.9
Dark clasts					
γ3	En	2000 May	6.7 $\pm$ 1.6	3.2 $\pm$ 1.2	-0.4 ± 0.9

[a] The external errors are included for $\delta^{18}O$ and $\delta^{17}O$ of individual analyses, while those of $\Delta^{17}O$ are only internal errors (see text for explanation). The mean values of repeated analyses for the same samples are the weighted mean (calculation by using the ISOPLOT program by Ludwig, 1998). The mean values of $\delta^{17}O$ are calculated from $\delta^{18}O$ and $\Delta^{17}O$ by applying the equation $\delta^{17}O = \Delta^{17}O + 0.52 \times \delta^{18}O$.

[b] Data obtained by using 25 μm primary ion beam was not included in the calculation of the mean $\delta^{18}O$ value because we did not evaluate reproducibility of $\delta^{18}O$ values of standards for the same condition.

magnesian clast α37A is the most ^{16}O-rich among all the clasts measured in this work that plot on the CCAM line. The $\Delta^{17}O$ value of the clast was analyzed more precisely by using a 25 μm primary beam with increased primary and secondary ion current. The result is $\Delta^{17}O = -2.2 \pm 0.3$‰ (2σ), which is at

the low end of the monomict ureilite data. The magnesian olivine-orthopyroxene clast might have been produced in a similar way as the monomict ureilites that formed from a relatively ^{16}O-rich and FeO-poor precursor.

Ureilitic mafic clasts in DaG-319 (including both type I and
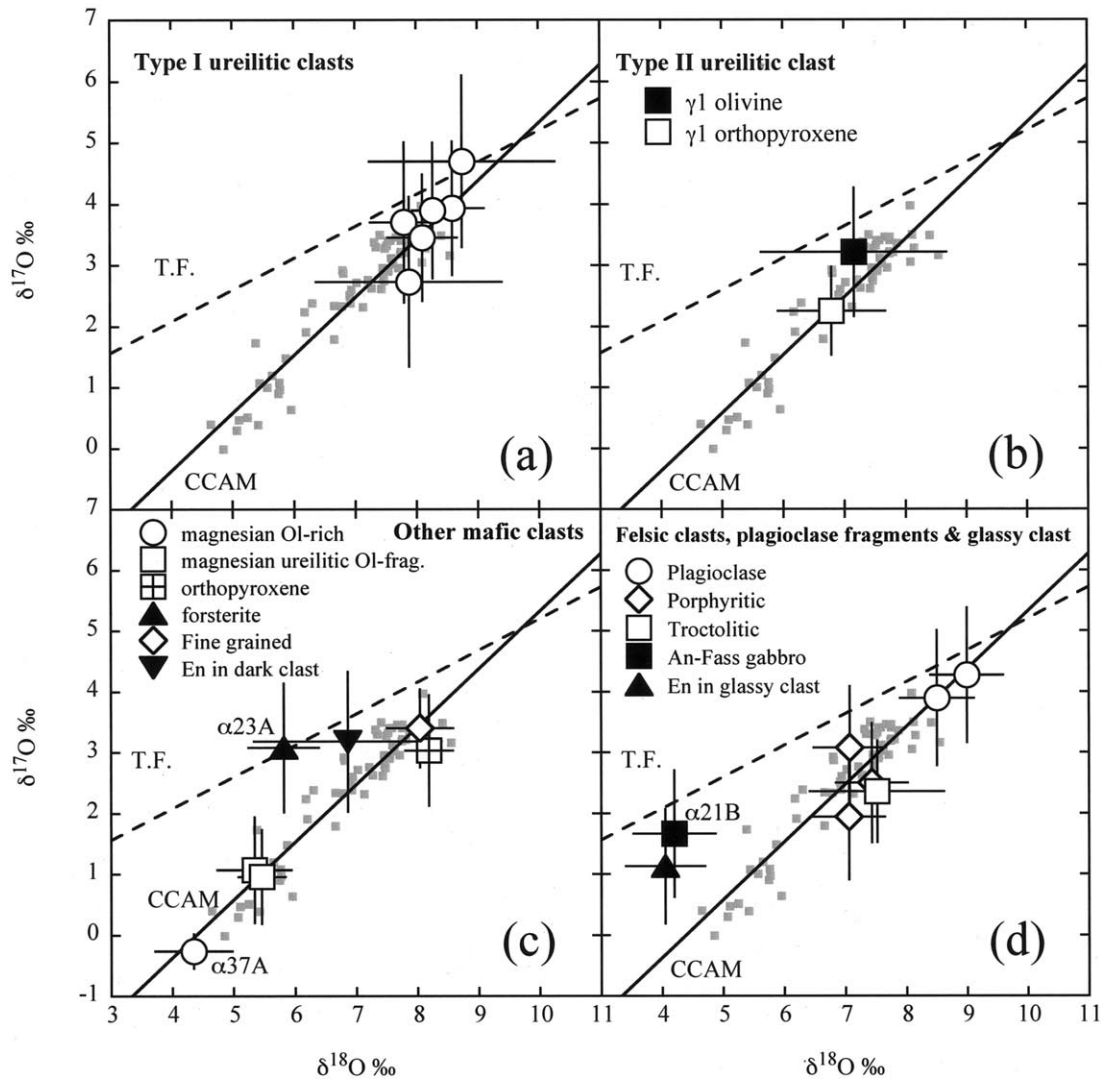
Fig. 3. SIMS oxygen isotope analyses of minerals in DaG-319 clasts. Small grey squares are literature data for monomict ureilites from Clayton and Mayeda (1988, 1996). (a) Type I ureilitic clasts. All data are obtained from olivine. (b) Type II ureilitic clasts. (c) Other mafic clasts and mafic mineral fragments. (d) Felsic clasts, plagioclase fragments, and glassy clasts. Error bars (in 2σ) include the external errors estimated from reproducibility of terrestrial standards in each analytical session. For duplicated analyses on minerals in each clast, the weighted average and the errors are shown.

type II ureilitic clasts) show the full ranges of mg# and $\Delta^{17}O$ that have been observed among the monomict ureilites. The fact that a single polymict ureilite contains ureilitic clasts with various $\Delta^{17}O$ supports the suggestion that all monomict ureilites are derived from a single parent body (Clayton and Mayeda, 1988).

Isolated orthopyroxene grain α20A is similar to orthopyroxene in the type II clast. Its oxygen isotopic composition is also similar to the type II clast γ1 (Figs. 3 and 4). The isolated forsterite grain α23A does not plot on the CCAM line and its $\Delta^{17}O$ is zero. This forsterite grain is probably not from the UPB. The fine-grained olivine clast α8B consists of granular olivine (mg#~79) with interstitial pigeonites and alkali-free glass. The oxygen isotopic composition and its mg#-$\Delta^{17}O$ relationship is exactly the same as those of the monomict ureilites. This is consistent with the origin of the fine-grained

clast α8B by shock melting of monomict ureilite-like material (Ikeda et al., 2000).

3.2.4. Porphyritic felsic clast, plagioclase fragments, and gabbroic clasts

We analyzed plagioclase and/or coexisting mafic minerals in 6 plagioclase-bearing felsic clasts. Because of a small grain size, reversely zoned pyroxene rims were not analyzed. We assume coexisting minerals to be in oxygen isotopic equilibrium. Plagioclase and pigeonite inclusions in α34A have same $\Delta^{17}O$ values within the analytical uncertainty. All data except a gabbroic clast (α21B) plot along the CCAM line (Fig. 3d), indicating that the plagioclase-bearing clasts were derived from the same precursors as the monomict ureilites. Their $\Delta^{17}O$ values typically range from -0.5‰ to -1.5‰, consistent with
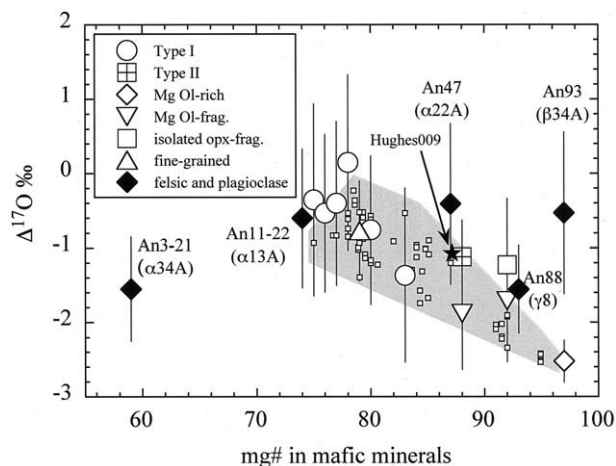
Fig. 4. The relationship between $\Delta^{17}O$ values and mg# of mafic minerals in individual clasts in DAG-319. Clasts with ureilitic origin, in which $\delta^{18}O$-$\delta^{17}O$ values plot along CCAM line, are shown. The ^{16}O enrichment is expressed as depletion in $\Delta^{17}O$ value. The mean value of $\Delta^{17}O$ is shown for each clast. Monomict ureilite data (small squares in the shaded area) are from Clayton and Mayeda (1988, 1996), including unusual monomict ureilite Hughes 009 shown as a solid star in comparison. Plagioclase bearing clasts deviate from the monomict ureilite trend significantly.

the majority of monomict ureilites. Although some of them contain high mg# (>90) mafic minerals, none of them plot in the range of the magnesian monomict ureilites ($\Delta^{17}O \leq -2‰$). There is no relationship between $\Delta^{17}O$ values and plagioclase compositions among these clasts; for example, $\alpha 13A$ (An$_{11}$-An$_{22}$), $\alpha 34A$ (An$_2$-An$_{21}$), and $\gamma 8$ (An$_{88}$) show similar oxygen isotopic compositions. However, there is a tendency for calcic plagioclase-bearing clasts to shift to the higher mg# side and albitic plagioclase bearing clasts toward the lower side.

Prinz et al. (1983, 1987) suggested that the anorthite-bearing clasts in North Haig and Nilpena (Jaques and Fitzgerald, 1982) are related to the Angra Dos Reis (ADOR) angrite. Clast $\alpha 21B$ is similar to the ADOR-related clast with respect to plagioclase compositions (An$_{98}$-An$_{100}$) and clinopyroxene compositions

Table 4. The $\Delta^{17}O$ values of minerals in DaG-319 clasts.

Sample	Mineral	Session	$\Delta^{17}O$	Error (2σ)
$\alpha 16A$	Olivine (Fo84)	2000 Aug	0.6	±0.8
$\beta 9B$	Magnetite	2000 Aug	2.7	±1.3
		2000 Aug	1.2	±2.3
		2000 Aug	3.2	±1.1
		weighted mean	2.8	±0.8
$\alpha 27A$	Fayalite	2001 Mar	4.4	±1.0
$\alpha 27A$	Olivine in basaltic clast-1	2000 Aug	−1.4	±1.2
$\alpha 27A$	Olivine in basaltic clast-2	2001 Mar	1.0	±1.1
$\alpha 27A$	Olivine in peridotitic clast	2000 Aug	2.7	±1.2
		2000 Aug	2.3	±1.1
		2000 Aug	1.1	±0.8
		2000 Aug	1.9	±0.9
		weighted mean	1.8	±0.5

(20–23% CaO, 5–6% Al$_2$O$_3$, ~1% TiO$_2$, 10–12% FeO). The oxygen isotopic composition of $\alpha 21B$ (Fig. 3d) is similar to the angrites ($\delta^{18}O$=3.7‰ and $\delta^{17}O$=1.8‰; Clayton and Mayeda, 1996), indicating that these clasts could be derived from the angrite parent body. Angrites are rare in the world's meteorite collections and therefore their occurrence as clasts in polymict ureilites is perplexing. Two other calcic plagioclase-bearing clasts ($\gamma 8$ and $\beta 34A$) have ureilitic oxygen isotopic signatures. These two clasts are associated with olivine or augite with high mg# (>90; Ikeda et al., 2000), while the ADOR-related clasts have olivine and clinopyroxene with low mg# (50–70; Prinz et al, 1986). Thus, the in situ oxygen isotopic measurements suggest that some calcic plagioclase-bearing clasts ($\gamma 8$, $\beta 34A$) in the DaG-319 polymict ureilite may be related to the monomict ureilites, while other calcic plagioclase-bearing clasts ($\alpha 21B$) are angritic.

3.2.5. Glassy clasts

The oxygen isotopic compositions of olivine or pyroxene in the glassy clasts $\alpha 8A$ and $\alpha 16A$ were measured. The analysis of olivine in $\alpha 16A$ was not stable so that only the $\Delta^{17}O$ value was obtained (Table 4); it is slightly higher compared to the monomict ureilites. Enstatite in clast $\alpha 8A$ has an oxygen isotopic composition that deviates slightly to the left of the CCAM line (Fig. 3d). Because of the small grain size in this clast, we could not make duplicate analyses. Therefore, it is not clear if the deviation of the data from CCAM line is an analytical artifact or real.

3.2.6. Dark clasts

Bulk oxygen isotopic compositions of some dark clasts in Nilpina polymict ureilite indicate that they plot on the extension of the CCAM line (Clayton and Mayeda, 1988). We determined the oxygen isotopic compositions of anhydrous minerals in dark clasts of DaG-319. Dark clast $\gamma 3$ contains several anhydrous mineral fragments set in a phyllosilicate-rich matrix. The anhydrous minerals could be part of the dark clast or grains that were mechanically mixed into the soft phyllosilicate clast during lithification of DaG-319. One analysis of an enstatite grain in $\gamma 3$ plots very close to the CCAM line (Fig. 3c), suggesting that the anhydrous minerals are of ureilitic origin. Another dark clast, $\alpha 27A$, contains basaltic and peridotic fragments set in a Fa-bearing phyllosilicate matrix. As groundmass of the basalt has suffered hydration, the basaltic fragments in $\alpha 27A$ might have brought into the dark clast before hydration. The $\delta^{18}O$ values in all the analyses from this clast (including data for olivines Fo$_{75-100}$ in lithic fragments and a fayalite grain in the matrix) drifted significantly, probably due to poor conductivity of the host fine-grained clast, so that only $\Delta^{17}O$ values were obtained. Fayalitic olivine in the matrix shows high $\Delta^{17}O$ values (~4‰), indicating the existence of a ^{16}O-depleted water component as in the case of the Nilpena CI-like dark clast (Clayton and Mayeda, 1988). The $\Delta^{17}O$ values of olivine in lithic fragments show a wide range (−1.4‰, 1‰ and 1.8‰), which may be due to in situ hydration by ^{16}O-depleted water, within the host (Ikeda et al., 2000). We also measured framboidal magnetites in the dark clast $\beta 9B$. However, the analyses were not stable, as in the case of clast

Table 5. Trace elements concentrations in plagioclase (in ppm, unless indicated).

Clast	Type	An-EPMA	An-SIMS	K (%)	Mg	Sc	Ti	V[a]	Cr[a]	Mn	Fe (%)	Co	Ni[a]	Cu[a]	Rb[a]	Sr	Ba
γ18	Fragment	95–97	90	0.0022	1,320	0.08	19	58	5.9	16	0.018	0.10	0.26	0.2	0.06	221	0.24
			90	0.0021	1,130	0.08	23	58	4.8	15	0.012	0.05	0.49	0.1	0.05	211	0.26
γ8	Troctolitic	87–89	85	0.0010	1,820	0.05	1.5	58	26	39	0.038	0.21		1.3		220	0.15
			84	0.0007	2,130	0.06	2.3	64	45	34	0.041	0.01		0.4		224	0.32
α32C	Porphyritic	36–60	57	0.083	960	0.27	250	17	7	155	0.35	0.27		0.8		207	14
			46	0.073	1,600	0.46	420	37	11	147	0.66	13.2	373	7.6	0.6	186	16
α22A	Fragment	47	46	0.024	1,740	0.02	56	38	18	53	0.079	0.79		7.8		276	8
			47	0.023	1,380	0.09	52	38	16	45	0.035	0.12		0.7		273	7
α23B	Fragment	36	35	0.027	920	0.11	107	18	8	43	0.032	0.01		0.8		222	10
α20B	Fragment	28–40	39	0.160	600	0.12	450	11	2.9	70	0.177	0.96		1.8		201	30
			35	0.177	630	0.14	540	10	4.7	74	0.185	1.50		41		196	28
			31	0.22	430	0.13	540	12	2.9	44	0.058	0.04		58		189	29
α13A	Porphyritic	22	22	0.198	380	0.11	520	8	1.6	31	0.048	0.02		0.9		156	34
γ5	Porphyritic	11–17	18	0.24		0.17	470	12	1.7							136	39
			18	0.173	529	0.14	500	16	2.9	29	0.090	3.6	54	0.5	0.7	113	37
α34A	Porphyritic	2–20	14	0.41	580	0.23	390	10	1.8	73	0.23	6.2		5.8		111	44
			4.7	0.33	114	0.08	580	4	0.3	9	0.041	0.005		0.6		44	39
			4.9	0.37	109	0.09	580	3	0.4	11	0.052	0.006		0.7		45	40
			4.9	0.48	155	0.10	610	4	0.3	25	0.123	1.32		1.6		46	43
			5.2	0.38	99	0.09	620	4	0.4	11	0.049	0.004		0.2		46	43
α19A	Porphyritic	10	6.9	0.25	880	0.26	660	9	1.6	73	0.143	15.1		5.2		75	42
			6.9	0.26	730	0.24	650	9	1.4	51	0.119	11.0		5.8		74	40
γ15	Porphyritic	2–9	3.6	0.39	53	0.08	590	7	0.5	5.1	0.035	0.01	0.12	0.2	3.2	57	42
			2.1	0.42	161	0.07	490	6	0.9	9.0	0.074	0.26	7.4	0.1	3.8	33	25
			1.8	0.47	89	0.06	460	4	0.3	5.0	0.050	0.09	1.5	0.2	4.0	31	24
α21A	Porphyritic	2	1.2	0.62	76	0.07	450	20	1.0	5.4	0.080	0.07	1.0	0.3	4.1	22	34

[a] Concentrations in plagioclase are estimated by applying relative sensitivity factors of V/Ti, Cr/Mn, Cu/Fe, Ni/Fe and Rb/K from glass standards. An-EPMA and An-SIMS are anorthite compositions of plagioclase from EPMA and SIMS data. SIMS An data are estimated from Na/Si and Ca/Si ratios during analyses.

α27A. The average $\Delta^{17}O$ value of the magnetite is 2.8 $\pm$ 0.8‰. In both α27A and β9B, minerals produced by hydration showed significantly higher $\Delta^{17}O$ values than that of the bulk analysis of CI-like dark clast in Nilpena ($\Delta^{17}O$ =1.49‰; Clayton and Mayeda, 1988). Considering that the dark clasts may contain minerals or fragments with lower $\Delta^{17}O$ values, oxygen isotopic composition of the water responsible for the formation of hydrated minerals and their associated phases should be extremely depleted in ^{16}O, at the level of $\Delta^{17}O \sim$ 3–4‰.

4. TRACE ELEMENT RESULTS

4.1. Trace Element Abundances in Plagioclase

The trace element concentrations of plagioclase in felsic clasts and plagioclase fragments were obtained by using SIMS. The results are shown in Table 5 and are plotted against anorthite content (mole %) in Figure 5. We could not measure anorthite in the "angritic clast" α21B because of its small size. The trace element concentrations show systematic variations; with increasing An content (1) K, Ti and Ba decrease, (2) Mg, V, Cr, and Sr increase, and (3) Sc and Fe show slight decrease. The Co and Cu concentrations show large scatter with no systematic variation in plagioclase composition. The systematic variations with An content in the plagioclase can be explained by fractional crystallization from a basaltic melt. However, the wide range of K, Ti and Ba in calcic plagioclase (An$_{>30}$) suggests that the calcic plagioclase is derived from different parental magmas with different incompatible trace element compositions.

In Figure 6, Mg/Fe ratios in plagioclase are compared to An contents and the mg# of coexisting mafic minerals. Clasts which are depleted in incompatible trace elements (K, Ti, and Ba) have systematically high Mg/Fe, indicating that their source magma had a higher mg# than the undepleted clasts. The clasts with high An content (An$_{>85}$, not including "angritic" plagioclase α21B) have the highest Mg/Fe ratios, and their coexisting mafic minerals have very high mg#s (93). In detail, the Mg/Fe ratios in plagioclase are significantly higher for the anorthitic plagioclase than the 1:1 relationship expected from other clasts with lower mg# (Fig. 6b). Partition coefficients for both Fe^{2+} and Fe^{3+} in plagioclase show stronger compositional dependencies than that of Mg (Bindeman et al., 1998). The significantly high Mg/Fe ratios in anorthitic plagioclase may be due to increased relative partitioning of Mg to Fe. Nonetheless, it is clear that the trace element depleted clasts are derived from high mg# magma sources. It should be noted that the oxygen isotopic compositions of the anorthitic plagioclase plot in the upper region of the CCAM line compared to those of the magnesian monomict ureilites (mg# = 90–95, see Figs. 3c,d).

4.2. Estimate of Parent Magma Compositions

By applying plagioclase/melt partition coefficients, concentrations of Mg, K, Ti, Sr, and Ba in the parental magma of the plagioclase bearing clasts were estimated. The experimental plagioclase/melt partition coefficients for these elements are well determined by Bindeman et al. (1998) that were used in the calculation. Because the partition coefficient data were
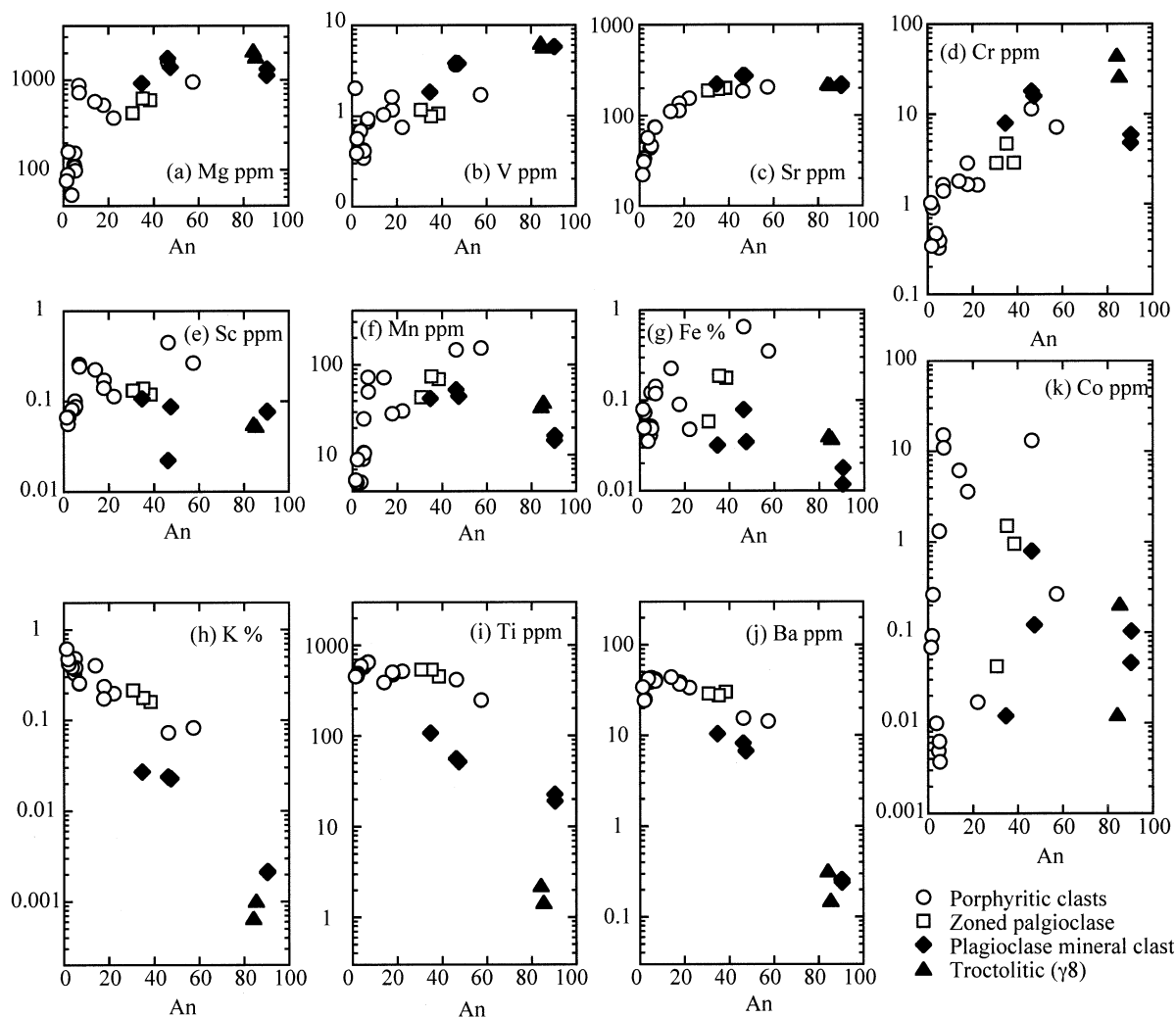
Fig. 5. Trace element abundances of plagioclase in DaG-319 clasts. (a) Mg ppm, (b) V ppm, (c) Sr ppm, (d) Cr ppm, (e) Sc ppm, (f) Mn ppm, (g) Fe %, (h) K %, (i) Ti ppm, (j) Ba ppm, (k) Co ppm. Open circles: porphyritic clasts, open squares: a single plagioclase with significant compositional zoning (α20B), solid diamonds: plagioclase mineral clasts, and solid triangles: troctolitic clast (γ8). The data represent the results of single spot analyses.

obtained from calcic plagioclase ($An_{>45}$), parental magma compositions were calculated for clasts with $An_{>45}$ plagioclase only. The results of the calculation are given in Figure 7 and show a systematic variation in CI normalized Ti, K, Ba, and Sr abundances with respect to the incompatibilities of the elements. The result from a porphyritic felsic clast (α32C) shows a relatively flat CI normalized abundance, while the others are systematically depleted in Ti, K, and Ba. Ti behaves as if it is less compatible than K in Figure 7a. The estimated MgO concentrations (wt%), the most compatible major element, also vary significantly from 4 to 18% and are inversely correlated with Ti, K and Ba depletion.

The estimated magma compositions for two anorthitic clasts (γ8 and γ18) are highly depleted in Ti, K, and Ba showing levels that are near-CI abundance or lower, while Sr concentrations are high, ~30 times CI abundance (Fig. 7a). The low Ti, K, and Ba concentrations in the melt indicate that the source regions were highly depleted in those elements. A selective depletion of incompatible trace elements in the source might

occur by the extraction of incompatible-rich melts from the source region prior to the final partial melting event. High Sr abundances restrict the degree of earlier partial melting to much less than 20%, at which point plagioclase is not completely exhausted from the chondritic precursor. This process may explain the anorthitic compositions for plagioclase in γ8 (An_{88}) and γ8 (An_{96}), because the low degree partial melt is enriched in albitic compositions. Furthermore, the estimated MgO contents of the parent magma are significantly high, up to 18% in γ8 (Fig. 7b). This also suggests that the mafic magma was produced by the repeated removal of basaltic components from the chondritic precursor. Ikeda and Prinz (2001) proposed fractional melting of a chondritic precursor for the origin of the UPB, in order to explain both the wide range of plagioclase compositions in the polymict ureilites and the olivine-pigeonite mineralogy of the monomict ureilite as the final residue. Our incompatible trace elements data provide clear evidence for fractional melting on the UPB.

The significantly large light REE (LREE) depletion in a melt
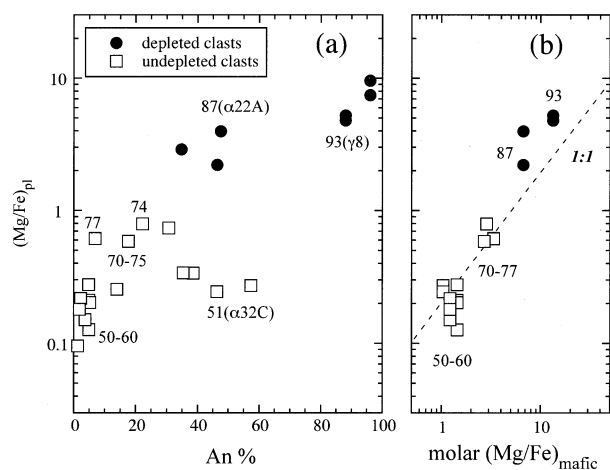
Fig. 6. Mg/Fe ratios of plagioclase in DaG-319. (a) anorthite contents versus Mg/Fe ratios. (b) molar Mg/Fe ratios in mafic minerals versus Mg/Fe ratios in coexisting plagioclase. "Depleted clasts" (solid circles) indicate incompatible trace elements (K, Ba and Ti) and "undepleted clasts" (open squares) indicate others clasts. Numbers near the symbols are mg# of the coexisting olivine and pyroxene.

clast in North Haig (Guan and Crozaz, 2001) and a melt inclusion in Hughes 009 (Goodrich et al., 2000), suggests that their parental magmas were derived from a fractionated precursor depleted in LREEs. As mentioned previously, Hughes 009 is a monomict ureilite with a mineralogy and petrology similar to that of the type II ureilitic clast γ1 in DaG-319. It is likely that their parental magmas were derived from partial melting of a depleted source, as in the case of the anorthitic plagioclase bearing clasts discussed above.

4.3. Trace Elements in Glass

The trace element concentrations of glass in glassy clasts and felsic clasts were also obtained and are shown in Table 6 and Figure 8. Alkali element abundances in glasses from felsic
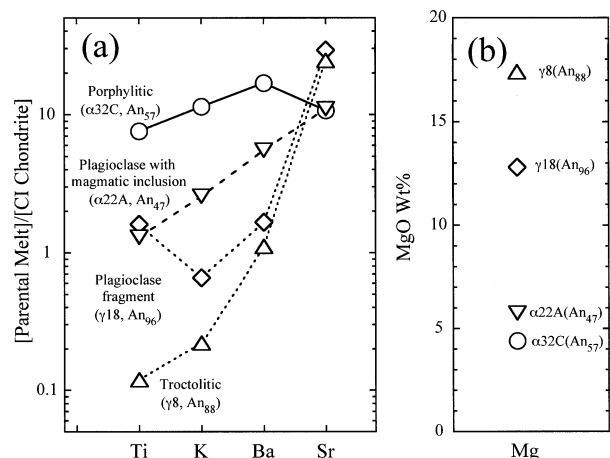
Fig. 7. Compositions of the estimated parental magma of the plagioclase bearing clasts. Partition coefficients of trace elements are from Bindeman et al. (1998). (a) CI normalized Ti, K, Ba and Sr abundance. (b) MgO%.

clasts (α21A and γ15) are high (10–200 × CI abundance) and are fractionated (Rb > K > Na), indicating that they formed after extensive fractional crystallization. The magnesian glassy clast (α8A) shows a relatively flat CI normalized abundance pattern for incompatible trace elements (Rb, K, Ba, Sr, and Na) and is highly depleted in siderophile elements. The clast might have formed by 10–20% partial melting of a chondritic precursor under significantly reducing condition. Low Ti abundance in this sample (Fig. 8) may indicate depletion of Ti from the glass by partitioning of Ti^{3+} into pyroxene. Another ferroan glassy clast (α16A) shows a trace element abundance pattern similar to that of glass in the albitic clasts, except that it is significantly depleted in alkali elements and but enriched in Sr, V and Cr. Although these clasts all contain glass with high SiO_2 (63~70%), a genetic relationship between the glassy clasts and felsic clasts is not clear. If the glassy clasts formed by partial melting of chondritic precursors similar to the monomict ureilites, α8A must have formed under highly reducing conditions and α16A formed from a more alkali-depleted precursor, compared to the conditions of ureilitic magma generation.

5. PARTIAL MELTING OF THE CHONDRITIC PRECURSOR

Here, trace element modeling for partial melting of the chondritic precursor is presented in order to better understand igneous processes on the UPB. We used Sr, Ba, and K concentrations in the estimated parental magma for the plagioclase-bearing clasts to test the model. These elements are mainly partitioned into plagioclase and the partition coefficients strongly depend on An contents. Therefore, the concentrations of Sr, Ba, and K are very sensitive to the amount and composition of plagioclase left in the solid source and its composition. We applied the MELTS program (Ghiorso and Sack, 1995; Asimow and Ghiorso, 1998) to obtain partial melting parameters, such as degree of melting, and plagioclase abundance and composition. In order to compare fractional melting with equilibrium partial melting, trace element model calculations were made for both batch melting and repeated 5% fractional melting. We examined other cases for the fractional melting model, such as repeated 1% and 10% melting conditions, but the results are similar to each other. Therefore, only the 5% fractional melting case is presented for simplicity.

Our ultimate goal is to understand the genesis of ultramafic monomict ureilite as the residual solid of the partial melting process. Distribution of Fe between silicate, metal and sulfide should be taken into account for the full understanding of the process, as it results in variations of mg# among different ureilites (e.g., Singletary and Grove, 2003). However, the present model deals with only the evolution of the silicate portion of the UPB, as the trace elements discussed here are strongly lithophilic elements. The mg# of the bulk silicates UPB is treated as one of the model parameter.

5.1. Starting Compositions and Partial Melting Conditions

The oxygen isotopic compositions and trace element compositions strongly indicate that the plagioclase-bearing clasts were derived from alkali-undepleted carbonaceous chondritic precursors. As we modeled the evolution of silicate portions,

Table 6. SIMS major and trace element analyses of glass in glassy and felsic clasts in DaG-319.

Sample	Magnesian glassy clast α8A		Ferroan glassy clast α16A		Porphyritic clast α21A				Porphyritic clast γ15	
	SIMS	EPMA*	SIMS	EPMA*	SIMS #1	SIMS #2	SIMS mean	EPMA* (this work)	SIMS	EPMA[a]
SiO_2 (%)	=70	70.07	=62.3	62.32	=70	=70	=70	69.27	=70	70.34
TiO_2 (%)	0.16	0.08	0.48	0.60	1.07	1.10	1.09	1.49	0.84	1.41
Al_2O_3 (%)	14.2	13.6	12.2	12.4	10.6	10.8	10.7	9.80	13.5	12.52
Cr_2O_3 (%)	0.005	0.00	0.067	0.26	0.01	0.01	0.01	0.10	0.01	0.08
FeO (%)	0.012	0.14	15.7	12.93	8.7	8.1	8.4	7.74	2.5	3.92
MnO (%)	0.025	0.00	0.57	0.11	0.57	0.55	0.56	0.14	0.15	0.00
MgO (%)	3.8	3.07	1.1	0.75	0.84	0.93	0.89	0.69	0.48	0.55
CaO (%)	4.9	3.79	7.9	8.08	0.88	0.96	0.92	0.99	0.39	0.31
Na_2O (%)	6.6	7.41	1.05	1.15	8.0	7.8	7.9	6.39	5.0	8.75
K_2O (%)	0.95	0.74	0.18	0.16	2.2	2.5	2.4	2.02	5.1	1.27
Sc (ppm)	24		18		11	12	12		6.2	
V (ppm)	1.8		11.2		1.4	2.0	1.7		2.5	
Co (ppm)	0.005		3.5		1.7	3.2	2.5		7.7	
Ni (ppm)	0.24		25		8	51	30		112	
Cu (ppm)	1.2		4.6		2.2	1.9	2.0		8.1	
Rb (ppm)	35		4.6		134	147	141		402	
Sr (ppm)	128		52		11	15	13		18	
Ba (ppm)	38		13		40	47	43		41	

[a] EPMA data is from Ikeda et al. (2000), except for α21A. The SiO_2 % is taken from EPMA analysis of each clast, which is used to calculate concentrations of major and trace elements from SIMS ($M+/^{28}Si+$) signal ratios.

we calculated volatile and Fe-FeS free bulk compositions from CI and CM carbonaceous chondrites whole rock data (Table 7; Anders and Grevesse, 1989, for CI and compilation by Lodders and Fegley, 1998, for CM). The amount of FeO in the precursor is estimated by assuming the mg# of the bulk precursor to be 77 and 90, which are in the range of those in monomict ureilites (74–95). The remaining Fe is removed as Fe-FeS components from bulk compositions. These estimates result in 1.5–2.0 × CI for lithophile element abundances in the starting materials, because bulk CI chondrite composition contains 30 wt % of water in hydrated minerals, organic matters, carbonates and

sulfates in addition to ~10% of estimated Fe-FeS components, which are not accounted for in the anhydrous silicate starting material. As shown in Table 7, initial plagioclase content and its chemical composition are calculated using the bulk Al_2O_3, Na_2O and K_2O compositions of the starting material. We assumed that 10% of bulk Al_2O_3 located in nonplagioclase phases, probably in pyroxene, because the bulk Al_2O_3 contents of the ultramafic monomict ureilites are in the range of 0.1 times of CI chondritic abundance.

From these starting compositions, we calculated the degree of melting (x), amount of plagioclase in the residual solid (p), and plagioclase An compositions (X_{An}) using the MELTS program with varied temperature (Appendix 3). Oxygen fugacity was set to 1.5 log unit below the iron-wüstite buffer. For the fractional melting model, we calculated p and X_{An} for 5% partial melting repeatedly by changing the starting compositions. The new starting composition for each step was calculated from the composition of the residual solid in the previous melting step. The results are summarized in Figure 9. Differences in the starting materials and melting conditions (batch or fractional) do not affect the amount of plagioclase in the solid residue. Differences in starting compositions (CI or CM) affect anorthite content (mole %) of the plagioclase significantly, because of different levels of Na. There is little difference between oxidized (mg#77) and reduced (mg#90) starting compositions. Fractional melting effectively increases the anorthite content as the melting is repeated, though the deviation from batch melting is not significant when the total melt fraction is less than 10%.

We recognize that the chemical compositions of calculated melts for less than 10% melting are extremely high in SiO_2% (>60%) and Na_2O/Al_2O_3 (>1) compared to those expected from the phase diagram of Fo44-An31-Qz (Longhi and Pan, 1989). There might be some unknown effects in calculating
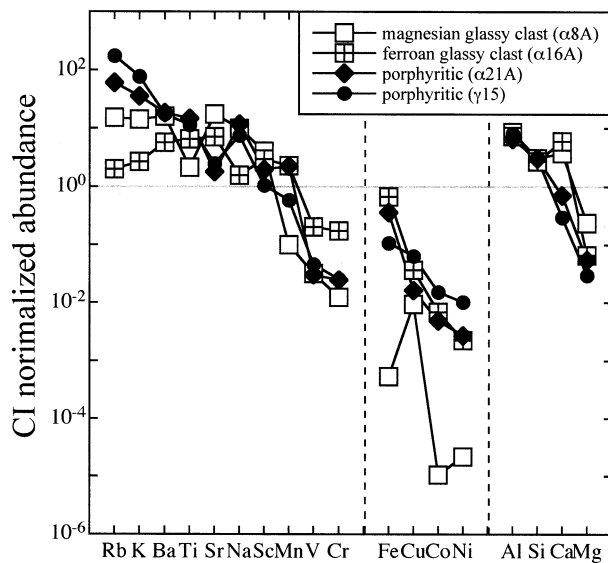
Fig. 8. CI normalized abundances of major and trace elements in the glass phase of DaG-319 clasts.

Table 7. Anhydrous, Fe-FeS free initial compositions.

Composition mg#	CI silicate compositions		CM silicate compositions	CI chondrite[a]	CM chondrite[a]
	77	90	77	46	45
SiO$_2$%	43.52	48.62	44.06	22.76	27.17
TiO$_2$%	0.139	0.155	0.149	0.073	0.092
Al$_2$O$_3$%	3.13	3.50	3.46	1.64	2.13
FeO%	16.70[b]	6.94[b]	16.47[b]	24.49	27.40
CrO%	0.74	0.83	0.72	0.39	0.45
MnO%	0.50	0.55	0.35	0.26	0.21
MgO%	31.36	35.04	30.93	16.40	19.07
CaO%	2.48	2.77	2.93	1.30	1.80
Na$_2$O%	1.29	1.44	0.85	0.67	0.53
K$_2$O%	0.129	0.144	0.072	0.067	0.045
Sr ppm	14.9	16.7	16.5	7.8	10
Ba ppm	4.47	5.00	4.94	2.34	3.1
plagioclase%[c]	13.2	14.7	12.1		
An	11.1	11.1	35.6		
Ab	83.5	83.5	61.0		
Or	5.5	5.5	3.4		

[a] CI and CM chondrite data are obtained from Anders and Grevesse (1989) and Lodders and Fegley (1998), respectively, recalculated to oxide% for major elements including Fe as FeO.

[b] FeO% of the initial compositions are estimated by adjusting bulk mg#.

[c] Plagioclase wt% and compositions are calculated from bulk Al$_2$O$_3$, Na$_2$O and K$_2$O contents by assuming 10% of bulk Al$_2$O$_3$ locates in nonplagioclase phases.

high albitic compositions (An$_{<30}$) in the MELTS program. Because the Na$_2$O/Al$_2$O$_3$ ratios in low degree partial melts may be overestimated, the estimated X_{An} in solid would be overestimated as well. The result of 1% partial melting of CI starting composition in the MELTS program is $p = 13\%$ $X_{An} = 0.16$, which is relatively high in X_{An} compared to the initial composition of $X_{An} = 0.11$ estimated in Table 7. For this reason, we extrapolated X_{An} towards $X_{An} = 0.11$ at 0% melting for less than 10% partial melting of the CI starting compositions (Fig. 9b). Plagioclase abundance was applied from the calculation result, as there is little difference between the MELTS calculation and the initial compositions in Table 7.

The major element compositions of the residual solids and liquids and the mineral compositions of the residual solid in the model calculations are shown in Appendix 3. In all model calculations, solid residues are highly depleted in Na$_2$O and Al$_2$O$_3$ when the total amount of liquid reaches 20%, at the point that plagioclase is almost exhausted. Therefore, the final ultramafic residue in this calculation becomes low alkali with a super-chondritic Ca/Al composition, which is suitable for the precursor of ultramafic monomict ureilites (Goodrich, 1999). It should be noted that in the MELTS calculation pigeonite appears as a solid residue for CM starting composition, which is moderately depleted in alkali and enriched in aluminum relative to CI compositions.

5.2. Trace Element Modeling

The trace element concentrations in the melt (C_m) are calculated using bulk partition coefficients (D), partial melting degree (x), and initial elemental concentrations (C_0), as follows:

$$C_m = \frac{C_0}{x + D(1 - x)}, \quad (1)$$

where

$$D = C_S/C_m, \qquad C_0 = xC_m + (1 - x)C_S$$

In the above equation, C_S indicates trace element concentration in the residual solid. In batch melting, C_0 is chosen as that of the starting composition and C_m varies with partial melting degree, x. In fractional melting, we assume that the melt component in each stage is removed from the system. Then, C_0 in the Nth stage melting is taken as the concentration of the element in the solid residue of the $(N - 1)$-th stage.

$$C_0^N = C_S^{N-1} = DC_m^{N-1} \quad (2)$$

The concentration of elements in a melt at a certain melting stage depends not only on x, but also on the number of previous melting steps and x in previous steps.

The bulk partition coefficients of K, Ba, and Sr are functions of the modal abundance of plagioclase (p) and plagioclase compositions (X_{An}) in the solid,

$$D = pD_{pl}(X_{An}) \quad (3)$$

where $D_{pl}(X_{An})$ is the plagioclase/melt partition coefficient of elements experimentally obtained by Bindeman et al. (1998). As the experimental data is obtained for $X_{An} > 45$, the $D_{pl}(X_{An})$ for albitic plagioclase are the extrapolated values. Other parameters p and X_{An} are estimated in the previous section.

Trace element modeling for partial melting of chondritic precursors was carried out for four cases; batch melting and 5% fractional melting of both CI and CM chondrite starting compositions with mg#=77. Because there was little difference in parameters, p and X_{An}, between oxidized (mg#77) and reduced (mg#90) starting compositions, the calculation for a reduced starting composition was not performed. The results shown in Figure 10 clearly demonstrate the differ-
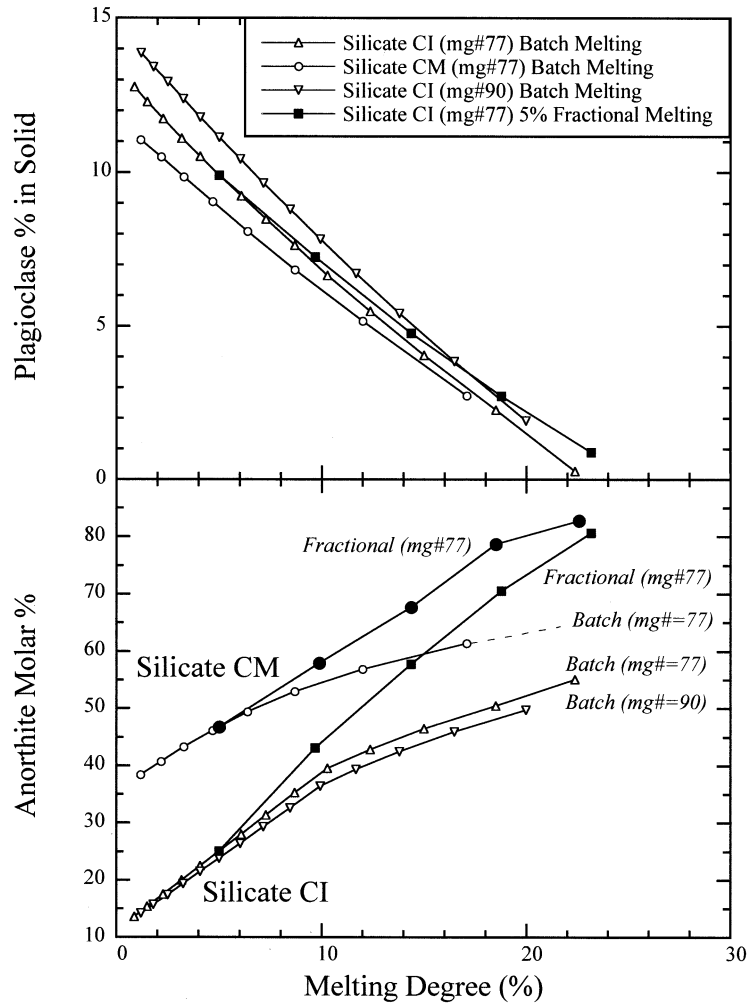
Fig. 9. Parameters of partial melting conditions obtained from the MELTS calculation. (a) Amount of plagioclase and (b) its composition in the residual solid versus melting degree. Melting degree represents cumulative melting fraction in the case of fractional melting calculations. Anorthite contents in plagioclase (b) for less than 10% partial melting of CI chondritic composition is extrapolated to An_{11} at 0% melting degree (solid line), which is estimated from the bulk compositions.

ence between batch melting and fractional melting. Low K and Ba concentrations in the magma can be produced only by fractional melting processes, while batch melting produces K and Ba enriched melt compositions. The results obtained for the fractional melting model match the data from DaG-319 clasts shown in Figure 7.

5.3. Formation of Plagioclase-Bearing Clasts on UPB

Trace element concentrations in plagioclase that crystallized from the magma are estimated as

$$C_{pl} = D_{pl}(X_{An})C_m \quad (4)$$

In Figure 11, C_{pl} from various models are compared to the measured data from DaG-319 plagioclase. Undepleted clasts with An = 30–60 are consistent with 10–20% batch melting of a CI chondrite starting material. The results of 5–10% batch melting of CM chondrite starting composition are also similar to undepleted clasts with An~50. Albitic clasts (An < 20)

show lower K contents than the model calculations of low degree of partial melting (<10%). The primary magma for albitic clasts might be produced by 10–20% batch melting of a CI chondritic precursor or 5–10% batch melting of CM chondritic precursor. Albitic clasts might be derived from an evolved magma after significant fractional crystallization. The oxygen isotopic compositions of ureilites range between CV3 matrix compositions and the intercept of CCAM line with the CI chondrite mass fractionation line. This also suggests that the precursor of ureilite had a more volatile rich chemical composition than CV chondrites. Therefore, according to both chemical compositions and oxygen compositions, we propose that the precursors of the UPB were alkali-rich carbonaceous chondrite materials with properties in between CV3 matrix and CI chondrites. Considering that abundant albitic plagioclase (<An20) among DaG-319 felsic clasts, CI-like alkali-rich chondritic precursor is more preferable than CM-like chondritic precursor.

K and Sr values in 5% fractional melting model calculations
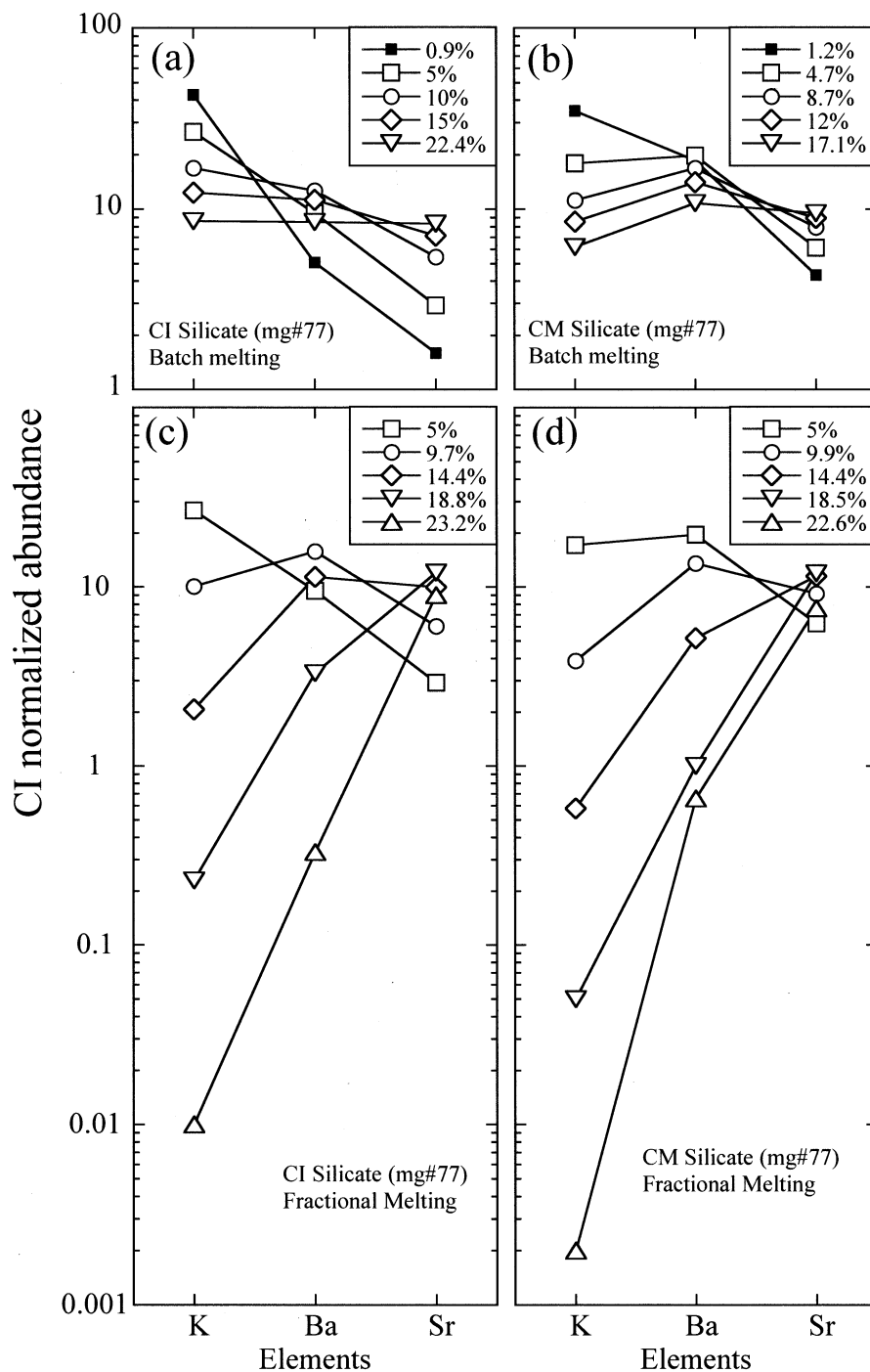
Fig. 10. Trace element abundances of melts during partial melting of a chondritic precursor. Abundances are normalized to CI chondrite. (a) batch melting of CI starting material, (b) batch melting of CM starting material, (c) 5% fractional melting of CI starting material, and (d) 5% fractional melting of CM starting material. In (c) and (d), the 5% fractional melting indicates repeated melt extraction from solid source. Since plagioclase composition and abundance in the partial melting model are not sensitive to mg# of the starting material, the case for which mg# = 77 in the starting material was examined. The fractional melting model matches the data from DaG-319 clasts shown in Figure 7.

are fairly similar to those of the depleted clasts shown in Figure 11. It should be noted that fractional melting calculation results are independent of starting conditions, as fractional melting effectively remove alkali from CI starting compositions. The concentration of Ba is more enriched than that of the batch melting model, so that the 5% fractional melting model does not reproduce the depleted Ba observed in plagioclase with moderate An compositions. This might be an artifact from the extrapolated Ba partition coefficients for albitic plagioclase, which are much higher than unity. Similar depletion trends for
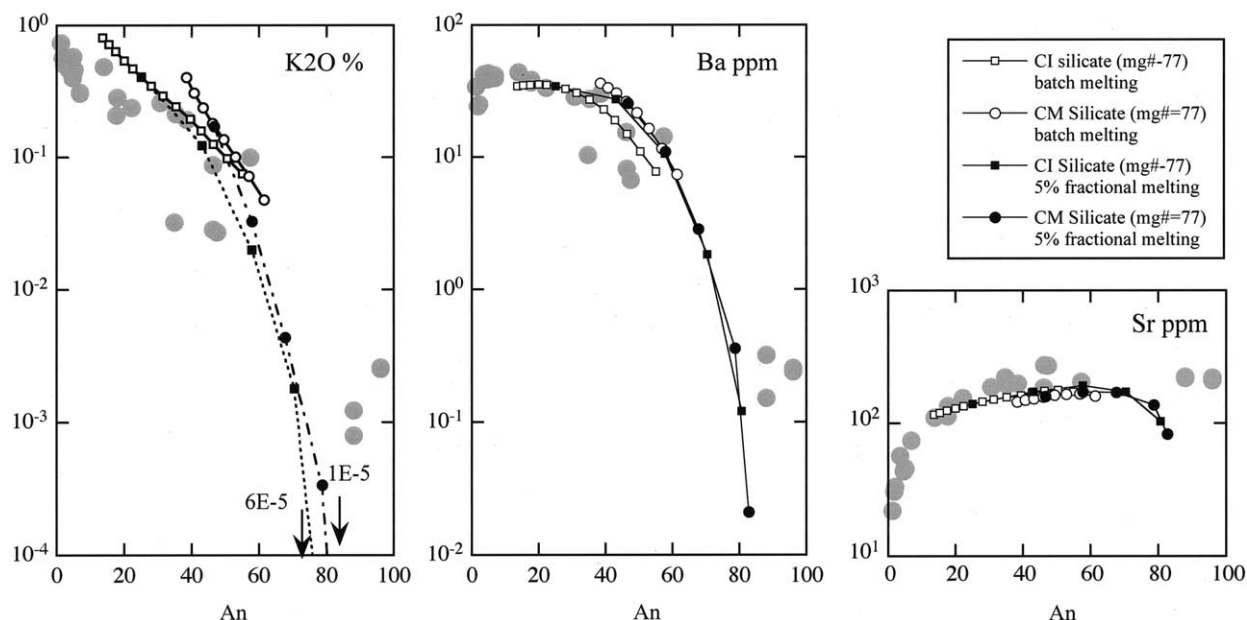
Fig. 11. Trace element concentrations in the plagioclase that crystallized from primary magma generated from partial melting of a chondritic precursor. Each data points correspond to partial melting parameters listed in Table A1. Undepleted clasts with moderate An (30–60) match well with batch melting of CI starting compositions, while depleted clasts generally match with fractional melting. Concentrations of K in albitic clasts cannot be reproduced in the model calculation.

K and Ba in plagioclase from depleted clasts (An ≥ 40; α22A, α23B, γ8, and γ18) indicate that the extrapolated Ba partition coefficients are overestimated. Anorthitic plagioclase bearing clasts may require more melting steps to reproduce their high An contents. However, increasing the number of melting steps would result in extreme depletions in K and Ba, suggesting that other effects, such as incomplete melt separation, should be considered to better match the model with the actual data with lesser depletion of incompatible elements. The model calculation failed to reproduce constant Sr concentration in anorthitic plagioclase (An > 80, Fig. 11). It reflects a small decrease in Sr partition coefficient with increasing An contents that is used in the above model. However, Togashi et al. (2000) indicated nearly constant Sr partition coefficients in plagioclase-basalt for An > 80. If we use the constant Sr partition coefficients, it is possible to reproduce constant Sr concentrations as we observed for DaG-319 clasts.

As described earlier, the anorthite contents of the plagioclase correlate with its Mg/Fe ratios, and the mg# of coexisting mafic minerals (olivine and pyroxene). The results of the MELTS calculation do not show significant mg# change (less than a few%) during fractional melting, so that the correlation of anorthite contents and Mg/Fe (Fig. 6a) may not be a result of the fractional melting process. The $\Delta^{17}O$ values in the anorthitic clasts are not as low as in the magnesian monomict ureilites (Fig. 4), indicating that they are not derived from the magnesian ureilite (mg# = 90–95) precursors. Therefore, the correlation between An content and mg# (or Mg/Fe ratios) cannot be explained without considering the effects of oxygen isotopic mixing with an ^{16}O-depleted reservoir, or reduction of FeO from the parental magma. If the mg# of monomict ureilites (i.e. residual solids) is controlled by smelting process as discussed by Singletary and Grove (2003), higher mg# for anorthic pla-

gioclase clasts may be explained by crystallization from upwelling magma where FeO is reduced to Fe-metal because of reduced pressure. Although metal is not observed among anorthitic clasts, the cumulate textures for these clasts indicate that the metal grains might be segregated from the system in the magma body.

From the above calculations, extremely low degree (<5%) partial melts enriched in K and Ba (>20 times CI abundance) could be produced in the early cycles of fractional melting (Fig. 10). These melts are the counterpart to the depleted source, which generated the K and Ba depleted magma. As shown in Figure 11, none of the clasts studied in this work from DaG-319 may be related to the magma produced by the extremely low partial melting degree. Therefore, the earliest enriched melts are missing in the polymict ureilites.

6. IMPLICATION FOR THE EVOLUTION OF UREILITE PARENT BODY

6.1. Formation of Olivine-Pigeonite Residue

The oxygen isotope and trace element compositions of the clasts in the DaG-319 polymict ureilite clearly show that the generation of magma on the UPB did not produce a global magma-ocean, but resulted in localized low degree partial melting. This process is key to understanding how the highly depleted ultramafic monomict ureilites formed. It is well known that monomict ureilites rarely contain aluminous silicate glass. This characteristic is very unusual if the ultramafic ureilites formed as solid residues from single stage large degree partial melting of a chondritic precursor. However, if the monomict ureilites formed after repeated episodes of small degree partial melting, the plagioclase components would be almost perfectly removed from the solid residue.

Goodrich (1999) suggested that the precursor of the ureilites should have super-chondritic Ca/Al ratios (2–3.5 × CI) if it formed by single-stage equilibrium partial melting. According to her equilibrium melting/crystallization calculation, partial melting of material with chondritic Ca/Al ratio would produce an olivine-orthopyroxene residue, not an olivine-pigeonite residue like monomict ureilites. Goodrich (1999) also mentioned that the precursor of the olivine-pigeonite ureilites should have low alkali contents because the orthopyroxene stability field expands at high alkali contents. Our MELTS calculation also indicated that batch melting of CI precursor would produce olivine-orthopyroxene residues (Appendix 3). As mentioned previously, CM starting composition would produce an olivine-pigeonite residue regardless of the melting models (batch or fractional). In addition, an olivine-pigeonite residue is also obtained from fractional melting of CI chondritic composition, though the amount of pigeonite is very limited (Appendix 3). The CaO/Al_2O_3 ratio in the residue becomes super chondritic (Ca/Al values >2.5) after plagioclase is exhausted. Therefore, fractional melting is effective in producing the olivine-pigeonite mineralogy of the mafic residues, even from alkali-rich chondritic precursors.

6.2. Missing Basalt Problem

According to our partial melting calculations, the total amount of melt generated to produce the parent magma of the plagioclase bearing clasts may be ~20%. From the chondritic precursor compositions, ~13% plagioclase content is expected for the whole parent body. However, there are no complementary basaltic meteorites to the ureilites among the more than 80 ureilites collected to date and the average abundance of plagioclase in the polymict ureilites is only a few % (Goodrich, 1999; Mittlefehldt et al., 1998). Therefore, the basaltic components are still largely missing among the present meteorite collections. As discussed earlier, an "enriched component" from a small degree partial melt should be produced in the early stages of fractional melting cycles, but is not observed among the plagioclase-bearing clasts in DaG-319. One possibility is that this component was lost by explosive volcanism from the UPB (e.g., Wilson and Keil, 1996). The early melts might have contained higher abundances of volatiles, so that the up-welling magma was efficiently lost to space. Another possibility is that the basaltic components were located near the surface of the parent body, they could have been selectively excavated into space by impacts. Nonetheless, the low abundance of plagioclase-bearing clasts among the polymict ureilites requires a process that will result in the loss of a large part of the magmatic component from the parent body. Thus, we rarely observe the small amount of early stage partial melt enriched in incompatible trace elements, while more depleted components were left in the parent body.

7. CONCLUSIONS

From in situ oxygen isotopic and trace element analyses of minerals in a variety of clasts in the DaG-319 polymict ureilite, we obtained the following conclusions;

(1) Oxygen isotopic compositions of olivine-pigeonite clasts with characteristic ureilitic carbon-metal veins (type I ureilitic clasts) are identical to those in monomict ureilites. Olivine-orthopyroxene-augite clasts without carbon-metal veins (type II ureilitic clasts) and other mafic clasts plot along the CCAM line, indicating their origin on the UPB. They show mg#-$\Delta^{17}O$ trends similar to those of the monomict ureilites. Magnesian clasts with high mg# (>90) olivine and pyroxene may be related to the magnesian monomict ureilites. Thus, a wide range of oxygen isotopic compositions, plotting along the CCAM line, is observed among clasts in a single polymict ureilite. This result supports previous suggestions that all ureilites were derived from a single parent body with heterogeneous oxygen isotopic compositions (Clayton and Mayeda, 1988).

(2) The $\Delta^{17}O$ value of the type II clast γ1 plots on the mg#-$\Delta^{17}O$ trend of monomict ureilites within analytical errors. This value is also consistent with that of the unusual monomict ureilite Hughes 009 and may support their common origin as suggested by Ikeda and Prinz (2001).

(3) Felsic clasts and plagioclase mineral clasts in DaG-319 plot on the CCAM line indicating that these clasts are derived from the basaltic magmas generated on the UPB. One exception is the clast containing anorthite and fassaite of angritic compositions; its oxygen composition plots near those of the angrites.

(4) The trace element abundances in plagioclase in the felsic clasts and plagioclase fragments in DaG-319 show systematic trends with anorthite contents. However, the incompatible trace element abundances (K, Ti and Ba) in the anorthitic clasts are extremely low and may require depleted magma sources. A comparison of trace element data with the partial melting model calculations indicates that the undepleted porphyritic clasts and zoned plagioclase clasts formed by batch melting (10–20%) of a chondritic precursor and subsequent fractional crystallization, while incompatible trace element depleted plagioclase-bearing clasts formed by fractional melting of a chondritic precursor. A CI and CM chondrite starting material best explains the variety observed in the albitic clasts.

(5) Alkali-rich carbonaceous chondrite material is the best potential candidate for the ureilite precursor, as the oxygen isotopic compositions of ureilites plot on CCAM line between CV3 matrix compositions and an extension of the CI chondrite mass fractionation line. Fractional melting may result in the depletion of albitic components in the solid residue. This residue may correspond to a precursor with super chondritic Ca/Al ratios that is required to produce the olivine-pigeonite ureilites by single stage partial melting (Goodrich, 1999).

REFERENCES

Anders E. and Grevesse N. (1989) Abundances of the elements—Meteoritic and solar. *Geochim. Cosmochim. Acta* 53, 197–214.

Asimow P. D. and Ghiorso M. S. (1998) Algorithmic modifications extending MELTS to calculate subsolidus phase relations. *Am. Mineral.* 83, 1127–1131.

Baertschi P. (1976) Absolute ^{18}O content of standard mean ocean water. *Earth Planet. Sci. Lett.* 31, 341–344.

Berkley J. L., Taylor G. J., Keil K., Harlow G. E., and Prinz M. (1980) The nature and origin of ureilites. *Geochim. Cosmochim. Acta* 44, 1579–1597.

Bindeman I. N., Davis A. M., and Drake M. J. (1998) Ion microprobe study of plagioclase-basalt partition experiments at natural concentration levels of trace elements. *Geochim. Cosmochim. Acta* 62, 1175–1193.

Boynton W. V., Starzyk P. M., and Schmitt R. A. (1976) Chemical evidence for the genesis of the ureilites, the achondrite Chassigny and the nakhlites. *Geochim. Cosmochim. Acta* 40, 1439–1447.

Choi B.-G., McKeegan K. D., Leshin L. A., and Wasson J. T. (1997) Origin of magnetite in oxidized CV chondrites: In situ measurement of oxygen isotope compositions of Allende magnetite and olivine. *Earth Planet. Sci. Lett.* 146, 337–349.

Clayton R. N. and Mayeda T. K. (1988) Formation of ureilites by nebular processes. *Geochim. Cosmochim. Acta* 52, 1313–1318.

Clayton R. N. and Mayeda T. K. (1991) Oxygen isotope studies of ordinary chondrites. *Geochim. Cosmochim. Acta* 55, 2317–2337.

Clayton R. N. and Mayeda T. K. (1996) Oxygen isotope studies of achondrites. *Geochim. Cosmochim. Acta* 60, 1999–2017.

Cohen B. A., Goodrich C. A., and Keil K. (2004) Feldspathic clast populations in polymict ureilites: Stalking the missing basalts from the ureilite parent body. *Geochim. Cosmochim. Acta,* in press.

Ghiorso M. S. and Sack R. O. (1995) Chemical mass transfer in magmatic processes. IV. A revised and internally consistent thermodynamic model for the interpolation and extrapolation of liquid-solid equilibria in magmatic systems at elevated temperatures and pressure. *Contrib. Mineral. Petrol.* 119, 197–212.

Goodrich C. A. (1992) Ureilites—A critical review. *Meteoritics* 27, 327–352.

Goodrich C. A. (1999) Are ureilites residues from partial melting of chondritic material? The answer from MAGPOX. *Meteorit. Planet. Sci.* 34, 109–119.

Goodrich C. A. and Jones J. H. (1987) Origin and evolution of the ureilite parent magmas—Multi-stage igneous activity on a large parent body. *Geochim. Cosmochim. Acta* 51, 2255–2273.

Goodrich C. A., Fioretti A. M., and Hoppe P. (2000) Rare Earth Elements in Primary Melt Inclusions in Olivine in Ureilite Hughes 009. *Lunar Planet. Sci.* **31,** 1192.

Goodrich C. A., Fioretti A. M., Tribaudino M., and Molin G. (2001) Primary trapped melt inclusions in olivine in the olivine-augite-orthopyroxene ureilite Hughes 009. *Geochim. Cosmochim. Acta* 65, 621–652.

Guan Y. and Crozaz G. (2001) Microdistributions and petrogenetic implications of rare earth elements in polymict ureilites. *Meteorit. Planet. Sci.* 36, 1039–1056.

Göbel R., Ott U., and Begemann F. (1978) On trapped noble gases in ureilites. *J. Geophys. Res.* 83, 855–867.

Ikeda Y., Prinz M., and Nehru C. E. (2000) Lithic and mineral clasts in Dar Al Gani (DAG) 319 polymict ureilite. *Antarct. Meteorite Res.* 13, 177–221.

Ikeda Y. and Prinz M. (2001) Magmatic inclusions and felsic clasts in the Dar al Gani 319 polymict ureilite. *Meteorit. Planet. Sci.* 36, 481–499.

Ikeda Y., Kita N. T., Morishita Y., and Weisberg M. K. (2003) Primitive clasts in the Dar al Gani 319 polymict ureilite: Precursors of the ureilites. *Antarct. Meteorite Res.* 16, 105–127.

Imai N., Terashima S., Itoh S., and Ando A. (1995) 1994 compilation of analytical data for minor and trace elements in seventeen GSJ geochemical reference samples, "Igneous rock series." *Geostandards Newsletter* 19, 135–213.

Jaques A. L. and Fitzgerald M. J. (1982) The Nilpena ureilite, an unusual polymict breccia—Implications for origin. *Geochim. Cosmochim. Acta* 46, 893–900.

Jochum K. P., Dingwell D. B., Rocholl A., Stoll B., Hofmann A. W., Becker S., Besmehn A., Bessette D., Dietze H. J., Dulski P., Erzinger J., Hellebrand E., Hoppe P., Horn I., Janssens K., Jenner G. A., Klein M., McDonough W. F., Maetz M., Mezger K., Munker C., Nikogosian I. K., Pickhardt C., Raczek I., Rhede D., Seufert H. M., Simakin S. G., Sobolev A. V., Spettel B., Straub S., Vincze L., Wallianos A., Weckwerth G., Weyer S., Wolf D., and Zimmer M. (2000) The preparation and preliminary characterisation of eight geological MPI-DING reference glasses for in-site microanalysis. *Geostand. Newsl.* 24, 87–133.

Kita et al. (2000) A short duration of chondrule formation in the solar nebula: Evidence from Al-26 in Semarkona ferromagnesian chondrules. *Geochim. Cosmochim. Acta* **64,** 3913–3922.

Lodders K. and Fegley B. (1998) *The Planetary Scientist Companion.* Oxford University Press. New York.

Longhi J. and Pan V. (1989) The parent magmas of the SNC meteorites. *Proc. Lunar Planet. Sci. Conf.* 19, 451–464.

Ludwig K. R. (1999) Using Isoplot/Ex, Version 2.01: A geochronological toolkit for Microsoft Excel. Special Publication No. 1a, 47. Berkeley Geochronology Center.

McKeegan K. D. (1987) Ion microprobe measurements of H, C, O, Mg, and Si isotopic abundances in individual interplanetary dust particles. Ph.D. thesis. Washington University, St. Louis.

Mittlefehldt D. W., McCoy T. J., Goodrich C. A., and Kracher A. (1998) Non-chondritic meteorites from asteroidal bodies. In *Reviews in Mineralogy: Planetary Materials*, Vol. 36 (ed. Papike J.). Washington, D.C.: Mineralogical Society of America. pp. 4-1–4-195.

Prinz M., Delaney J. S., Nehru C. E., and Weisberg M. K. (1983) Enclaves in Nilpena polymict ureilite (abstract). *Meteoritics* 18, 376–377.

Prinz M., Weisberg M. K., Nehru C. E., and Delaney J. S. (1986) North Haig and Nilpena: Paired polymict ureilites with angra DOS reis-related and other clasts. *Lunar Planet. Sci.* 17, 681–682.

Prinz M., Weisberg M. K., Nehru C. E., and Delaney J. S. (1987) EET 83309, A Polymict Ureilite: Recognition of a New Group. *Lunar Planet. Sci.* 18, 802–803.

Scott E. R. D., Taylor G. J., and Keil K. (1993) Origin of ureilite meteorites and implications for planetary accretion. *Geophys. Res. Lett.* 20, 415–418.

Singletary S. J. and Grove T. L. (2003) Early petrologic processes on the ureilite parent body. *Meteorit. Planet. Sci.* 38, 95–108.

Takeda H. (1987) Mineralogy of Antarctic ureilites and a working hypothesis for their origin and evolution. *Earth Planet. Sci. Lett.* 81, 358–370.

Togashi S., Kita N. T., and Morishita Y. (2000) Small degrees of partial melting for primitive magmas of lunar highland rocks estimated from trace elements in plagioclase. *Lunar Planet. Sci.* 31, 1537.

Togashi S., Kita N. T., Tomiya A., Morishita Y., and Imai N. (2003) Melt contribution to partitioning of trace element between plagioclase and basaltic magma of Fuji volcano, Japan. *Appl. Surf. Sci.* 203–204, 814–817.

Warren P. H. and Kallemeyn G. W. (1989) Geochemistry of polymict ureilite EET83309, and a partially-disruptive impact model for ureilite origin. *Meteoritics* 24, 233–246.

Warren P. H. and Kallemeyn G. W. (1992) Explosive volcanism and the graphite-oxygen fugacity buffer on the parent asteroid(s) of the ureilite meteorites. *Icarus* 100, 110–126.

Wilson L. and Keil K. (1996) Clast sizes of ejecta from explosive eruptions on asteroids: Implications for the fate of the basaltic products of differentiation. *Earth Planet. Sci. Lett.* 140, 191–200.

APPENDIX 1

Mass Spectrometric Conditions of Oxygen Isotopic Analyses

Secondary ion optics

The transfer optics was set to 30 μm image field, which corresponds to 200 times magnification from sample surface to the field aperture plane. The entrance slit width was set to 75 μm and the field aperture was opened to be 4000 μm square (equivalent to 20 μm square on sample surface). These secondary optical settings allow high ion transmission (>70%) at high mass resolution of 4500 (Kita et al., 2000). Energy slit was set at −5 eV for the lower edge with energy band width

of 35 eV. We carefully aligned the primary beam to be the center of the field aperture, in order to avoid possible instrumental mass fractionation effects related to the position of the ion image. Further, we carefully tune the immersion lens voltage (the first ion lens from the sample surface) to maximize the secondary ion intensity, which may correct the effect of the sample height as well as collection efficiency of the sputtered secondary ions.

Secondary ion detection

The secondary ions of ^{16}O (8×10^8 cps), ^{17}O (3×10^5 cps), and ^{18}O (2×10^6 cps) were detected simultaneously in the multicollection mode using three Faraday cup (FC) detectors; two mobile FC detectors with a fixed exit slit width for ^{16}O (10^{10} Ω) and ^{18}O (10^{11} Ω), and a mono-collector FC (axial FC) with an adjustable exit slit width for ^{17}O (10^{11} Ω). Amplifiers of multicollector FCs utilize those of Finnigan Mat, which is widely used for conventional mass spectrometers, and that of axial FC is equipped with optional Keithley Electrometer (Model 642). Both types of amplifiers are reliable for high precision isotopic analyses in terms of linearity, stable sensitivity, and low baseline drifts ($\sim 2 \times 10^{-16}$ A). The aberration of mass spectrum along the focal plane made it difficult to obtain a flat top mass spectrum for ^{16}O and ^{18}O for MRP $>$2000. However, the multicollection system does not allow us to chose different exit slit width for individual detectors. This is the reason why we combined mono-collector with adjustable exit slits in the multicollection mode, as the requirements for MRP that remove molecular interferences are $>$4500 for ^{17}O and $>$2000 for ^{16}O and ^{18}O. A single analysis consists of 40 cycles of measuring baseline mass (M = 16.8 at the axial detector; 10 s for both waiting time and measurement time) and oxygen isotopes (5 s for waiting time and 10 s for measuring time) by switching magnet and takes 25 min. The baseline measurement is critical for the accurate analyses as the baseline drifts of the FC detectors are in the range of $\sim$1000 cps (or 2×10^{-16}A) for 5 s integrations, which corresponds to 0.3% of the ^{17}O signals.

Electron gun

The normal incident electron gun was used for charge compensation. The electron gun was set to equi-potential to the sample voltage (-10 kV). The zero energy electrons are exposed as a shower ($\sim$100 μm diameters) on the sample surface, which may hit the sample if the sample voltage is shifted by the loss of secondary electrons from ion sputtering. The electron gun is tuned to maximize the sample current on the conductive material (such as Cu mesh on Al plate) by applying a 20 V offset to the sample voltage. The electron current to the sample surface is limited to 50 μA (20–30 μA on Cu-Al mesh) by adjusting the filament current to be 1.3 mA to avoid too many free electrons exposed to nearest lenses causing deformation of the secondary ion optics. The position of the electron beam is adjusted using magnetic coils (x and y directions) while looking at H ions from adsorbed water. The position is strictly adjusted to the center of the field aperture, where the primary ion beam should be located. With a small offset voltage ($<$5 V), a small bright spot ($\sim$20 μm) with a triangle shape is seen as the H ion image (Fig. A1, b). By maximizing the electron current, we usually see a symmetrical H ion image. The shape and position of electron beam is checked before the sample is exposed to the Cs primary ion beam. If the electron beam is not at the center of the field aperture, the position is adjusted by magnetic coils. If the shape of electron beam becomes less symmetric, the electrostatic deflectors are used to readjust the shape. If a sample is well polished and flat, the position-to-position adjustments are minor within a single mount or thin section. We see moderate differences among different mounts and thin sections.

This adjustment seems to provide a relatively focused electron beam to the sample surface with a similar size to the primary ion beam. Conventional adjustments are made to homogenize a large ($\sim$100 μm) H ion image by applying 20 V sample offset (similar to Fig. A1, c). The electron beam alignments in both the conventional method and the present work are only slightly different. We consider that the electron beam is always stronger at the center, even with the former method, though it is hardly recognized by observing the bright H ion image with 20 V offset voltages. We found the secondary oxygen ion yields are significantly higher (10–20%) and instrumental mass fractionation effects are smaller (a few ‰) by focusing the electron beam. It is likely that neutral oxygen atoms sputtered by the Cs primary ions are further negatively ionized by the electrons exposed to the sample surface. This
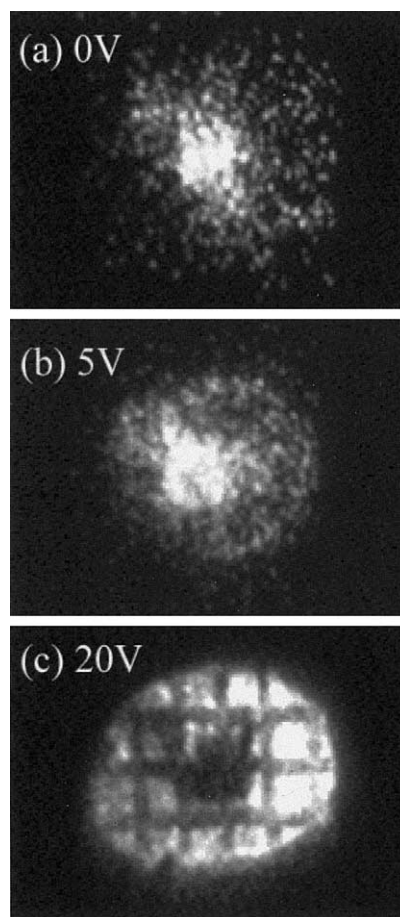
Fig. A1. The H ion image of the surface adsorbed water by electron gun. (a) H ion image without offset voltage appears only at the central $\sim$20 μm circle area. (b) With a small offset voltage ($<$5 eV), a $\sim$50 μm ring shape with a bright central spot is observed. The symmetric shape is carefully tuned by electron gun deflectors. (c) For the normal offset voltage (20 eV) to observing H ion image, a homogeneous oval shaped area (150 $\times$ 100 μm) is seen on 25 μm Cu grid on Al-mesh. The image was taken after a few minutes of electron exposure, and the central part (dark area) lost surface adsorbed water because of higher electron intensity at the center.

could be a reason why instrumental mass fractionation is very sensitive to electron gun adjustment.

APPENDIX 2

Oxygen Isotopic Analyses of Terrestrial Standards

The $(^{17}\text{O}/^{16}\text{O})_{\text{SMOW}}$ ratios of terrestrial standards are calculated for individual analyses as

$$(^{17}\text{O}/^{16}\text{O})_{\text{SMOW}} = (^{17}\text{O}/^{16}\text{O})_{\text{measured}} \times \left\{ 1 - 0.52 \times \frac{(\delta^{18}\text{O})_{\text{measured}}}{1000} \right\},$$

where

$$(\delta^{18}\text{O})_{\text{measured}} = \left\{ \frac{(^{18}\text{O}/^{16}\text{O})_{\text{measured}}}{(^{18}\text{O}/^{16}\text{O})_{\text{SMOW}}} - 1 \right\} \times 1000.$$

The results of all the terrestrial standards are shown in Figure A2. We do not see any variation in calculated $(^{17}\text{O}/^{16}\text{O})_{\text{SMOW}}$ ratios above analytical uncertainties. The mean values for May 2000 and July–August 2000 analytical sessions agree well within the uncertainties of
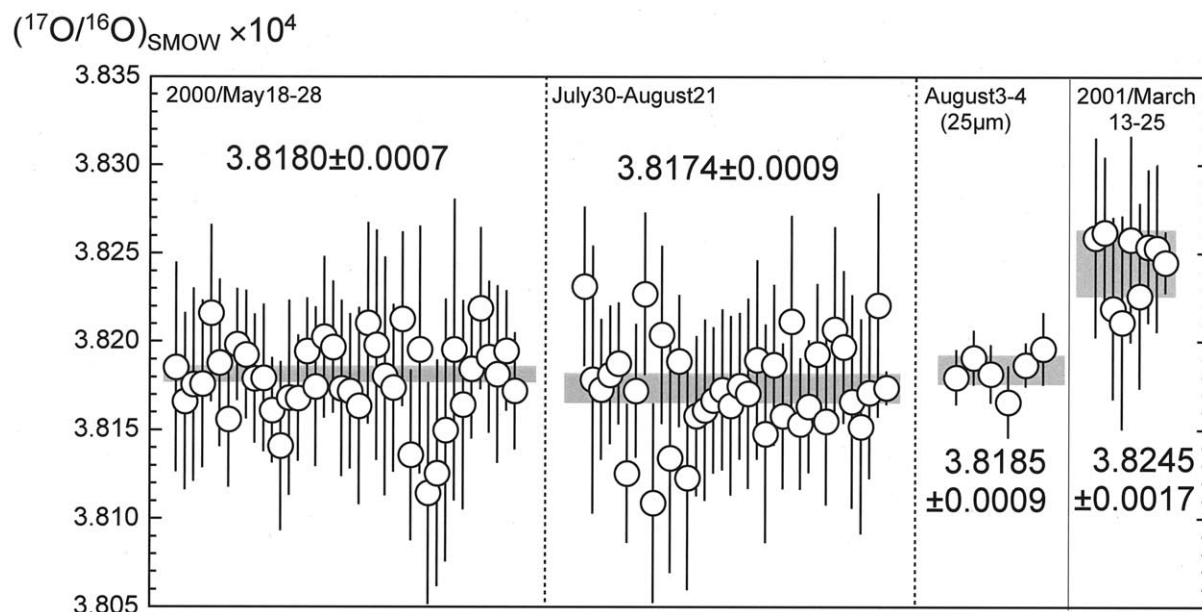
$(^{17}O/^{16}O)_{SMOW} \times 10^4$

Fig. A2. The $(^{17}O/^{16}O)_{SMOW}$ ratios of the terrestrial standards measured with Multicollection FC detectors. Error bars equated to data are 2σ level). The numbers equated to three data sets are the mean values and their errors multiplied by 10,000 for individual analytical sessions.

0.3‰. However, the mean value of ~3.818 × 10^{-4} is significantly lower than (3.831 ± 0.003) $\delta^{18}O$ values × 10^{-4} by McKeegan (1987). It may be possible that the ~3.4‰ lower SMOW $(^{17}O/^{16}O)$ ratios in our instrument was responsible for relative sensitivity between multi-collector and Mono-collector FC detectors. The multicollector system is equipped with a software to calibrate FC amplifiers by using reference currents of 9 × 10^{-11}A, though Mono-collector FC was not calibrated against multicollectors. In March 2001, by comparing ^{18}O signal in Mono collector FC and multicollector FC, the calibration was manually done for Mono-collector FC. The mean $(^{17}O/^{16}O)_{SMOW}$ ratios in this session was (3.825 ± 0.002) × 10^{-4}, which is closer to, but still 1.7 ± 0.9‰ lower than, the literature value.

The instrumental mass fractionation effects are evaluated by using the measured $\delta^{18}O$ values of terrestrial standards against the $\delta^{18}O$ values obtained by conventional gas mass spectrometry for the same samples, as follows;

$$f = (\delta^{18}O)_{measured} - (\delta^{18}O)_{conventional}$$

The reproducibility of f for individual standard often exceeds the internal precision of $(\delta^{18}O)$ data. The external error of f values range 0.6–2.0‰ and 0.3–1.1‰ for 2000 May and 2000 July-August session, respectively (Fig. A3). Sometime, only one or two data were obtained for each standard in a single day, it is difficult to evaluate external errors for each day. Therefore, external errors of 1.5‰ and 0.5‰ are assigned for f values of 2000 May and 2000 July-August session, respectively. The day-to-day variation of average f value for individual standard is normally within 1‰, though it shifted as much as 2‰ in some cases.

In March 2001 session, as we completed developing the routine adjustment procedure for e-gun, the reproducibility of the f value during standard analyses became significantly better. No external error is indicated from standard analyses.
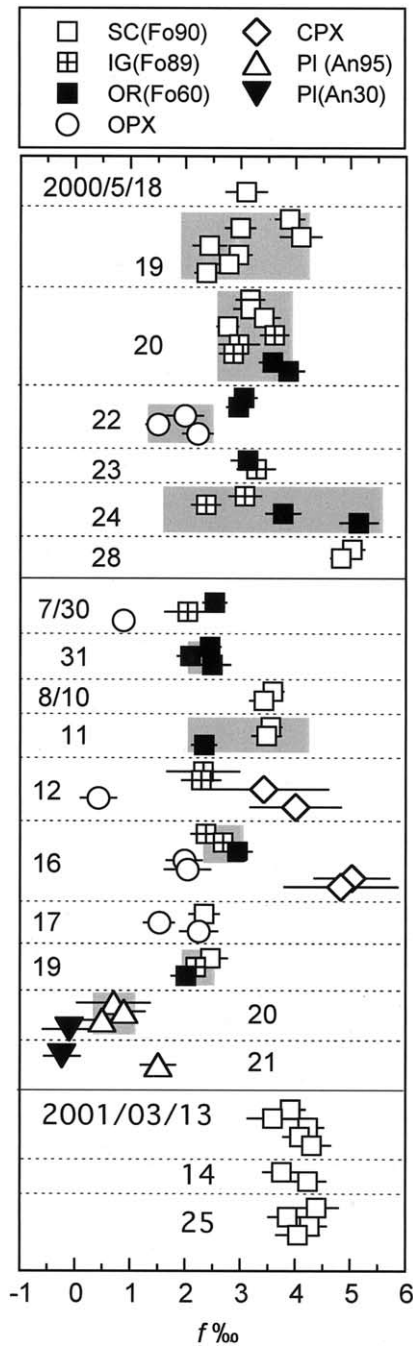
Fig. A3. Instrumental mass fractionation effects among terrestrial standards. Error bars for each data are internal error of the SIMS analyses. External errors of f values are calculated using ISOPLOT program (Ludwig, 1999) for standards data obtained for more than three times in a single day for the same minerals, which are shown as grey boxes. Two plagioclase standards with different An contents are treated as different minerals, while three olivine standards with different Fo contents are treated as same mineral because of lack of significant matrix effects on f values.

APPENDIX 3

Compositions of Melts and Residual Solid During the Partial Melting of the Chondritic Precursors Obtained from the MELTS Program

The results of major elements in melts and residual solids and mineral compositions in residual solids are shown in Table A1.

Table A1. Mineral and major element compositions of partial melting of chondritic precursor obtained from MELTS program.[a]

T (°C)	Melt[b] (%)	Mineral (%)					Composition of the melt (oxide wt%)										Composition of the residual solid (oxide wt%)									
		Ol	Opx	Pig	Aug	Pl	SiO_2	TiO_2	Al_2O_3	FeO	MnO	MgO	CaO	Na_2O	K_2O	CaO/Al_2O_3	SiO_2	TiO_2	Al_2O_3	FeO	MnO	MgO	CaO	Na_2O	K_2O	CaO/Al_2O_3
							CI silicate (mg# = 77) batch melting																			
1030	0.9	74	3.1	—	8.5	13	70.3	1.30	8.1	2.5	0.07	1.6	2.5	11.8	1.72	0.3	43.6	0.13	3.1	16.9	0.50	31.9	2.5	1.20	0.12	0.8
1040	1.5	74	3.3	—	8.2	12	69.5	1.46	8.6	2.7	0.07	1.7	2.8	11.3	1.77	0.3	43.4	0.12	3.1	17.0	0.51	32.1	2.5	1.14	0.10	0.8
1050	2.3	74	3.4	—	8.0	12	68.7	1.64	9.1	2.9	0.08	1.9	3.0	10.8	1.78	0.3	43.3	0.10	3.0	17.1	0.51	32.3	2.5	1.08	0.09	0.8
1060	3.2	74	3.5	—	7.6	11	67.8	1.85	9.6	3.1	0.09	2.0	3.4	10.3	1.74	0.4	43.1	0.08	2.9	17.2	0.51	32.6	2.5	1.00	0.08	0.8
1070	4.1	74	3.5	—	7.3	11	67.2	1.82	10.0	3.4	0.09	2.2	3.7	9.9	1.67	0.4	42.9	0.07	2.9	17.3	0.52	32.8	2.5	0.93	0.06	0.9
1080	5.0	74	3.4	—	7.0	10	66.7	1.71	10.4	3.6	0.10	2.3	4.0	9.6	1.57	0.4	42.6	0.06	2.8	17.5	0.52	33.1	2.4	0.86	0.05	0.9
1090	6.1	74	3.3	—	6.7	9.2	66.1	1.58	10.8	3.9	0.11	2.5	4.3	9.2	1.46	0.4	42.4	0.05	2.7	17.6	0.52	33.5	2.4	0.79	0.04	0.9
1100	7.3	74	3.1	—	6.4	8.5	65.5	1.44	11.1	4.2	0.12	2.7	4.6	8.8	1.34	0.4	42.2	0.04	2.5	17.8	0.53	33.9	2.3	0.71	0.04	0.9
1110	8.7	74	2.9	—	6.0	7.6	64.8	1.30	11.5	4.5	0.12	2.9	5.0	8.4	1.21	0.4	41.9	0.03	2.4	17.9	0.53	34.3	2.3	0.62	0.03	1.0
1120	10.3	74	2.5	—	5.6	6.7	64.1	1.16	11.9	4.9	0.13	3.2	5.4	8.0	1.08	0.5	41.5	0.02	2.2	18.1	0.54	34.9	2.2	0.53	0.02	1.0
1130	12.4	74	1.9	—	5.1	5.5	63.3	1.01	12.3	5.3	0.15	3.5	5.9	7.5	0.95	0.5	41.1	0.02	1.9	18.4	0.55	35.6	2.0	0.43	0.01	1.1
1140	15.0	74	1.1	—	4.4	4.1	62.4	0.87	12.7	5.7	0.16	3.8	6.5	6.9	0.81	0.5	40.6	0.01	1.5	18.7	0.56	36.5	1.8	0.31	0.01	1.2
1150	18.5	75	—	—	3.5	2.3	61.4	0.72	13.1	6.2	0.17	4.2	7.1	6.3	0.68	0.5	39.9	0.01	0.9	19.2	0.57	37.8	1.5	0.17	0.01	1.6
1160	22.4	75	—	—	1.8	0.3	59.9	0.61	13.5	6.8	0.18	4.7	7.9	5.7	0.58	0.6	39.2	0.00	0.2	19.7	0.59	39.3	0.9	0.03	0.00	5.0
1170	24.2	75	—	—	0.3	—	59.3	0.57	12.9	7.3	0.19	5.2	8.5	5.3	0.53	0.7	38.9	0.00	0.0	19.8	0.60	40.0	0.6	0.01	0.00	15
1180	24.7	75	—	—	—	—	59.0	0.56	12.7	7.7	0.20	5.4	8.5	5.2	0.52	0.7	38.9	0.00	0.0	19.8	0.60	40.2	0.5	0.01	0.00	17

CI silicate (mg# = 90) batch melting

1030	1.2	54	22	—	8.6	14	71.2	1.62	8.2	0.7	0.11	1.9	2.5	12.0	1.79	0.3	48.8	0.14	3.5	7.1	0.56	35.7	2.8	1.32	0.12	0.8
1040	1.8	54	22	—	8.3	13	70.8	1.63	8.6	0.7	0.12	2.1	2.7	11.6	1.82	0.3	48.6	0.13	3.4	7.1	0.57	35.9	2.8	1.26	0.11	0.8
1050	2.5	54	22	—	8.0	13	70.3	1.62	9.1	0.8	0.13	2.2	2.9	11.2	1.82	0.3	48.5	0.12	3.4	7.1	0.57	36.2	2.8	1.20	0.10	0.8
1060	3.3	55	22	—	7.7	12	69.8	1.59	9.5	0.8	0.14	2.3	3.1	10.9	1.80	0.3	48.3	0.11	3.3	7.2	0.57	36.4	2.8	1.13	0.09	0.8
1070	4.1	55	22	—	7.3	12	69.3	1.54	9.9	0.9	0.15	2.5	3.4	10.6	1.75	0.3	48.2	0.10	3.3	7.2	0.57	36.7	2.8	1.06	0.08	0.9
1080	5.0	55	22	—	7.0	11	68.9	1.48	10.3	0.9	0.16	2.7	3.7	10.2	1.67	0.4	48.0	0.09	3.2	7.3	0.58	37.1	2.8	0.99	0.06	0.9
1090	6.0	55	22	—	6.6	10	68.4	1.40	10.7	1.0	0.17	2.9	4.0	9.9	1.58	0.4	47.8	0.08	3.1	7.4	0.58	37.4	2.7	0.91	0.05	0.9
1100	7.2	55	22	—	6.2	9.7	67.9	1.32	11.1	1.1	0.18	3.1	4.3	9.6	1.47	0.4	47.6	0.07	2.9	7.4	0.59	37.8	2.7	0.83	0.04	0.9
1110	8.5	55	22	—	5.8	8.8	67.4	1.23	11.5	1.2	0.19	3.3	4.6	9.2	1.35	0.4	47.3	0.06	2.8	7.5	0.59	38.3	2.6	0.74	0.03	0.9
1120	10.0	55	22	—	5.3	7.8	66.8	1.13	12.0	1.3	0.21	3.6	5.1	8.8	1.23	0.4	47.1	0.05	2.6	7.6	0.60	38.8	2.5	0.64	0.03	1.0
1130	11.7	55	21	—	4.8	6.7	66.2	1.03	12.4	1.4	0.22	3.9	5.5	8.4	1.10	0.4	46.8	0.04	2.4	7.7	0.60	39.5	2.4	0.54	0.02	1.0
1140	13.8	56	21	—	4.3	5.4	65.5	0.93	12.8	1.5	0.24	4.2	6.0	7.9	0.97	0.5	46.4	0.03	2.0	7.9	0.61	40.3	2.3	0.42	0.01	1.1
1150	16.5	56	20	—	3.6	3.9	64.8	0.82	13.2	1.6	0.25	4.6	6.6	7.3	0.84	0.5	45.9	0.02	1.6	8.1	0.62	41.4	2.1	0.30	0.01	1.3
1160	20.0	57	18	—	2.7	1.9	64.0	0.71	13.7	1.7	0.27	5.0	7.2	6.7	0.71	0.5	45.3	0.02	1.0	8.3	0.63	42.9	1.7	0.15	0.00	1.7
1170	23.9	58	17	—	1.5	—	63.3	0.62	13.9	1.8	0.28	5.5	7.9	6.1	0.61	0.6	44.6	0.01	0.3	8.6	0.64	44.7	1.2	0.01	0.00	4.1
1180	25.3	59	16	—	0.2	—	63.2	0.60	13.3	2.0	0.28	5.9	8.4	5.7	0.57	0.6	44.3	0.01	0.2	8.7	0.65	45.3	0.9	0.00	0.00	4.0

CM silicate (mg# = 77) batch melting

1100	1.2	66	—	18	3.8	11	61.8	3.87	12.4	4.4	0.12	3.2	5.8	6.2	2.02	0.5	44.2	0.11	3.4	16.7	0.35	31.5	2.9	0.79	0.05	0.9
1110	2.2	66	—	18	3.1	10	61.7	3.27	12.5	4.8	0.13	3.4	6.1	6.3	1.66	0.5	44.0	0.08	3.3	16.8	0.36	31.8	2.9	0.74	0.04	0.9
1120	3.3	66	—	18	2.3	9.9	61.5	2.72	12.7	5.2	0.13	3.6	6.4	6.3	1.37	0.5	43.8	0.06	3.2	16.9	0.36	32.1	2.8	0.67	0.03	0.9
1130	4.7	66	—	18	1.4	9.1	61.1	2.25	12.8	5.6	0.14	3.9	6.8	6.2	1.12	0.5	43.6	0.05	3.0	17.1	0.36	32.5	2.8	0.60	0.02	0.9
1140	6.4	66	—	18	0.4	8.1	60.5	1.83	13.1	6.1	0.14	4.2	7.2	5.9	0.91	0.6	43.3	0.04	2.8	17.3	0.36	33.0	2.7	0.51	0.02	0.9
1150	8.7	66	—	17	—	6.8	59.8	1.46	13.3	6.6	0.15	4.5	7.7	5.5	0.72	0.6	42.9	0.02	2.5	17.5	0.37	33.7	2.5	0.42	0.01	1.0
1160	12.0	67	—	16	—	5.2	59.0	1.13	13.7	7.1	0.16	5.0	8.3	4.9	0.56	0.6	42.4	0.02	2.1	17.8	0.38	34.7	2.2	0.30	0.01	1.1
1170	17.1	67	—	12	—	2.7	58.1	0.83	14.0	7.6	0.17	5.5	8.9	4.3	0.41	0.6	41.6	0.01	1.3	18.4	0.39	36.4	1.7	0.16	0.00	1.3
1180	23.3	68	—	7.7	—	—	57.4	0.63	14.2	8.1	0.18	6.0	9.4	3.6	0.31	0.7	40.4	0.00	0.2	19.1	0.40	38.8	1.0	0.01	0.00	4.1
1190	24.7	69	—	5.8	—	—	57.4	0.60	13.6	8.5	0.18	6.4	9.5	3.4	0.29	0.7	40.1	0.00	0.2	19.2	0.41	39.3	0.8	0.01	0.00	4.6
1200	26.0	69	—	4.0	—	—	57.4	0.57	13.1	8.9	0.18	6.7	9.4	3.3	0.28	0.7	39.8	0.00	0.1	19.2	0.41	39.7	0.7	0.01	0.00	5.2

CI silicate (mg# = 77) 5% fractional melting

1080	5.0	70	3.2	—	6.7	9.4	66.7	1.71	10.4	3.6	0.10	2.3	4.0	9.6	1.57	0.4	42.6	0.06	2.8	17.5	0.52	33.1	2.4	0.86	0.05	0.9
1132	9.7	71	2.8	—	5.4	6.7	63.3	0.87	12.2	5.5	0.15	3.5	6.0	7.6	0.82	0.5	41.6	0.01	2.3	18.1	0.54	34.7	2.2	0.52	0.01	1.0
1168	14.4	71	—	3.6	2.5	4.2	59.4	0.25	13.4	7.6	0.21	5.1	8.4	5.3	0.23	0.6	40.6	0.00	1.7	18.7	0.56	36.3	1.9	0.25	0.00	1.1
1186	18.8	71	—	2.2	1.4	2.2	55.8	0.04	13.9	9.3	0.26	6.7	10.7	3.1	0.04	0.8	39.8	0.00	1.0	19.2	0.57	37.9	1.4	0.10	0.00	1.4
1194	23.2	71	—	—	0.7	0.5	53.4	0.01	14.1	10.3	0.30	7.9	12.3	1.5	0.01	0.9	39.0	0.00	0.3	19.7	0.59	39.6	0.8	0.02	0.00	3.0

CM silicate (mg# = 77) 5% fractional melting

1132	5.0	63	—	17	1.2	8.4	61.0	2.16	12.9	5.7	0.14	3.9	6.9	6.1	1.08	0.5	43.5	0.05	3.0	17.1	0.36	32.6	2.7	0.58	0.02	0.9
1166	9.9	63	—	16	—	5.9	58.9	0.68	13.6	7.6	0.17	5.2	8.4	5.0	0.32	0.6	42.7	0.01	2.4	17.7	0.37	34.1	2.4	0.34	0.00	1.0
1184	14.4	64	—	14	—	3.8	56.6	0.16	14.1	8.9	0.20	6.3	9.9	3.5	0.07	0.7	41.9	0.00	1.8	18.1	0.38	35.5	2.0	0.18	0.00	1.1
1193	18.5	64	—	11	—	2.0	54.8	0.04	14.6	9.7	0.22	7.3	11.0	2.2	0.00	0.8	41.3	0.00	1.2	18.6	0.39	37.0	1.6	0.07	0.00	1.4
1198	22.6	65	—	8.5	—	0.3	53.5	0.01	15.0	10.2	0.2	7.9	11.7	1.3	0.00	0.8	40.7	0.00	0.4	19.0	0.40	38.5	1.1	0.01	0.00	2.5

[a] CrO content is not considered as the MELTS program assumes trivalnent Cr.
[b] Melting (%) indicates equilibrium partial melting degree for batch melting and cumulative melt fractions for fractional melting.